N71-19021
NASA CR-116824

NATIONAL AERONAUTICS AND SPACE ADMINISTRATION

Technical Memorandum 33-455

Extraterrestrial Convergent Photogrammetric Mapping System — an Error Analysis

Milosh Benesh

CASE FILE COPY

JET PROPULSION LABORATORY
CALIFORNIA INSTITUTE OF TECHNOLOGY
PASADENA, CALIFORNIA

December 1, 1970

NATIONAL AERONAUTICS AND SPACE ADMINISTRATION

Technical Memorandum 33-455

Extraterrestrial Convergent Photogrammetric Mapping System — an Error Analysis

Milosh Benesh

JET PROPULSION LABORATORY
CALIFORNIA INSTITUTE OF TECHNOLOGY
PASADENA, CALIFORNIA

December 1, 1970

Prepared Under Contract No. NAS 7-100
National Aeronautics and Space Administration

Preface

The work described in this report was performed by the Space Sciences Division of the Jet Propulsion Laboratory.

Acknowledgment

The author wishes to express his appreciation to T. Bird for his help with the general outline of this project, as well as for his continuing technical and moral support. Special thanks are due to S. Seng for his cooperation on the analog test and for the photographic processing that was done with the greatest care possible. Expressions of appreciation are also made to T. Rindfleisch and R. Blackwell for their understanding and help with preparation of the simulated TV pictures, and to R. Becker for his help in editing and proofreading the manuscript.

Contents

Contents (contd)

Tables

Contents (contd)

Figures

Abstract

An effort to define specific photogrammetric parameters that could be incorporated into an extraterrestrial television mapping system through investigations of convergent photogrammetric stereomodels is described. Also described are error analyses of direct and external relative orientation, and practical tests that investigated: (1) aspects of TV image quality and its resulting influence upon mapping accuracy, and (2) the design of an effective analytical method for complex interior orientation calibration.

Extraterrestrial Convergent Photogrammetric Mapping System—an Error Analysis

I. Introduction

The long-range objective of this study is to provide definition of specific photogrammetric parameters that can be incorporated into the design of an orbital or flyby television system so that effective extraterrestrial mapping objectives may be satisfied.

The research itself is based on experience and results obtained from previous investigations (Refs. 1 and 2). In the application of photogrammetric requirements to orbiting and flyby television systems, it has been shown that a conventional parallel camera configuration can provide only limited capability. Because of adverse system limitations (i.e., small vidicon format, long focal length, limited photogrammetric image quality, etc.), in most of these cases, direct solution of the relative orientation problem is not possible and external orientation data must be used. Because of the lack of ground control points, the same applies to absolute orientation.

One solution to this problem is to use three-photo relative orientation instead of the conventional two-photo approach. This method has been discussed by many photogrammetrists (one of the best descriptions can be found in Ref. 3), but it has not found wide acceptance in photogrammetric practice, mainly because its accuracy improvement is not commensurable to the increased analytical effort (Ref. 4).

It was decided, therefore, to undertake analytical investigations of convergent camera configurations, which would enable a high base-to-height ratio and result in a simple and accurate mapping system without significantly reducing other imaging capabilities.

The first part of this project consists of modifications of the error analysis described in Refs. 1 and 2. This modification is necessary to satisfy the immediate objective of this study: definition of accuracies and tolerances required for the application of convergent photography for extraterrestrial mapping. This investigation is considered in relation to orbital or flyby altitudes and includes the influence of different image format–focal length–convergency and overlap combinations.

In the original approach to this problem, the interior orientation calibration errors (i.e., the focal length and the principal point eccentricity errors) were treated as any other random variables. However, unpublished research by the author shows that their influence is predominantly systematic despite their random origin. Therefore, to complete the study, it was necessary to analyze this systematic influence for similar parameter combinations as mentioned earlier.

An additional objective was to develop criteria required to establish optimum image quality and interior orientation parameters that uniquely qualify the spaceborne

television system for topographic mapping through the application of photogrammetric techniques.

This second part of the program objective has been met by utilizing laboratory studies for determination of image quality and interior orientation parameters for a television system. These tests involved application of a conventional stereometric camera system (Zeiss SMK-120) imaging a known accurate target field. Subsequent tests have utilized television scanning of the source target material to provide the required supporting data for the theoretical comparative investigations. Associated with these activities have been certain investigations regarding the effect of digital image processing on the overall photogrammetric capability of the system.

This information can then be used to develop image quality and calibration criteria that are controlling factors in the actual design of an ultimate mapping system. These factors have been described in terms of calibration requirements and accuracy tolerances, rather than specific procedures and techniques that are dependent upon the engineering design of a final system.

Final conclusions of this study consider the compatibility of the recommended configurations in relation to data reduction and map production capabilities.

The program can thus be divided into four basic research steps:

(1) Error analysis of the direct and external relative orientation (considering the influence of image format–focal length–convergency and overlap combinations).

(2) Analysis of the systematic interior orientation calibration errors (considering the influence of image format–focal length–principal point eccentricity and convergency combinations).

(3) Image quality (considering the influence of resolution, random noise, reseau mark quality, photometric and geometric distortions, digital processing, etc.).

(4) Interior orientation camera calibration (i.e., definition of complex camera system geometric distortions, correct focal length, and principal point eccentricity).

Some of these problems have already been described and briefly discussed (Ref. 5); however, in the interest of completeness and clarity, the most important results and aspects will be repeated here.

The general purpose of the research activities was twofold:

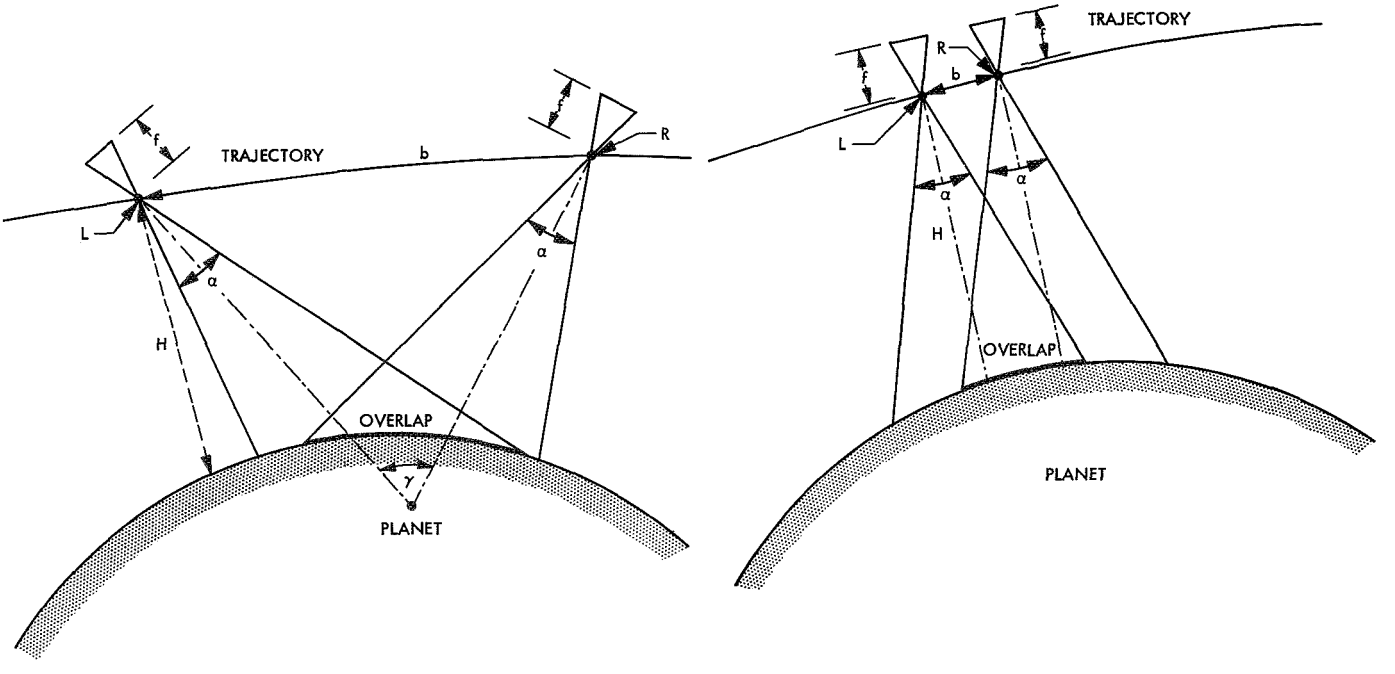

Fig. 1. Photogrammetric mapping systems

(1) To define the parameters of an optimum photogrammetric mapping system without concern for any existing state-of-the-art constraints.

(2) Same as in (1), assuming some general constraints that are compatible with the *Mariner* Mars 1969 and *Mariner* Mars 1971 missions.

In neither case, however, was there any intention to change existing photogrammetric or computational hardware or to design a new system.

II. Convergent Photogrammetry

The difference between a convergent and a normal (parallel) photogrammetric case is apparent from Fig. 1. It can clearly be seen that convergent photography results in a considerably improved base-to-height ratio, which is very favorable. However, there are certain undesirable constraints and limitations connected with this improvement, and these have a detrimental effect upon the final mapping accuracy or upon the general applicability of this method.

One of the limitations of convergent photography is that many conventional analog photogrammetric instruments are not equipped to accommodate large angles of convergency. However, analytical image evaluation and data reduction using a mono- or stereocomparator are absolutely unrestricted and unlimited in this respect.

It must also be realized that, compared to a normal case, convergent photogrammetry involves much more complicated mathematical relations; however, with the availability of efficient electronic computers, this should not represent any serious problem.

The greatest problem of convergent photography is the continuously changing image scale along the flight direction. This can considerably influence the mapping accuracy, particularly in cases of larger image formats and/or short focal lengths.

To define an optimum convergent photogrammetric system enabling not only an improved base-to-height ratio, but a considerably increased mapping accuracy as well, it was necessary to consider all the aforementioned factors and to analyze all their influences.

There is, of course, an unlimited number of convergency–overlap combinations that could be investigated. To obtain a realistic sample, the following parameters were chosen:

Convergency	$\gamma = 40, 80, 120$ deg
Overlap	Hundred percent overlap (HPO), negative overlap (NO), and positive overlap (PO)

For a given convergency γ, the desired overlap combination can be obtained by an appropriate change of the stereophotogrammetric base. These three basic combinations, which are shown in Fig. 2, represent the most significant convergent cases:

Hundred percent overlap	Complete maximum coverage of both images with relatively large scale differences
Negative overlap	Shorter base results in a relatively small overlap; however, areas with the largest scale factor are utilized
Positive overlap	Longer base gives the best base-to-height ratio possible; however, only areas with the smallest scale factor are covered

Before any further computations were made, a FORTRAN program was written to enable parameter determination of all the required convergency–overlap combinations.

The following symbols were used (Fig. 2):

x, y = image coordinates in camera system

$f = -z$ = focal length

O', O'' = left and right camera center of projection

b = stereophotogrammetric base

γ = angle of convergency

ψ = camera angle of coverage

$\bar{x}, \bar{y}, \bar{z}$ = image coordinates transformed into a system parallel with the ground coordinate system

X, Y, Z = ground coordinates (Z is flight height)

Inasmuch as all computations are based on fictitious model data, the ground projection of each image format must be determined. This is done in two steps: first, the

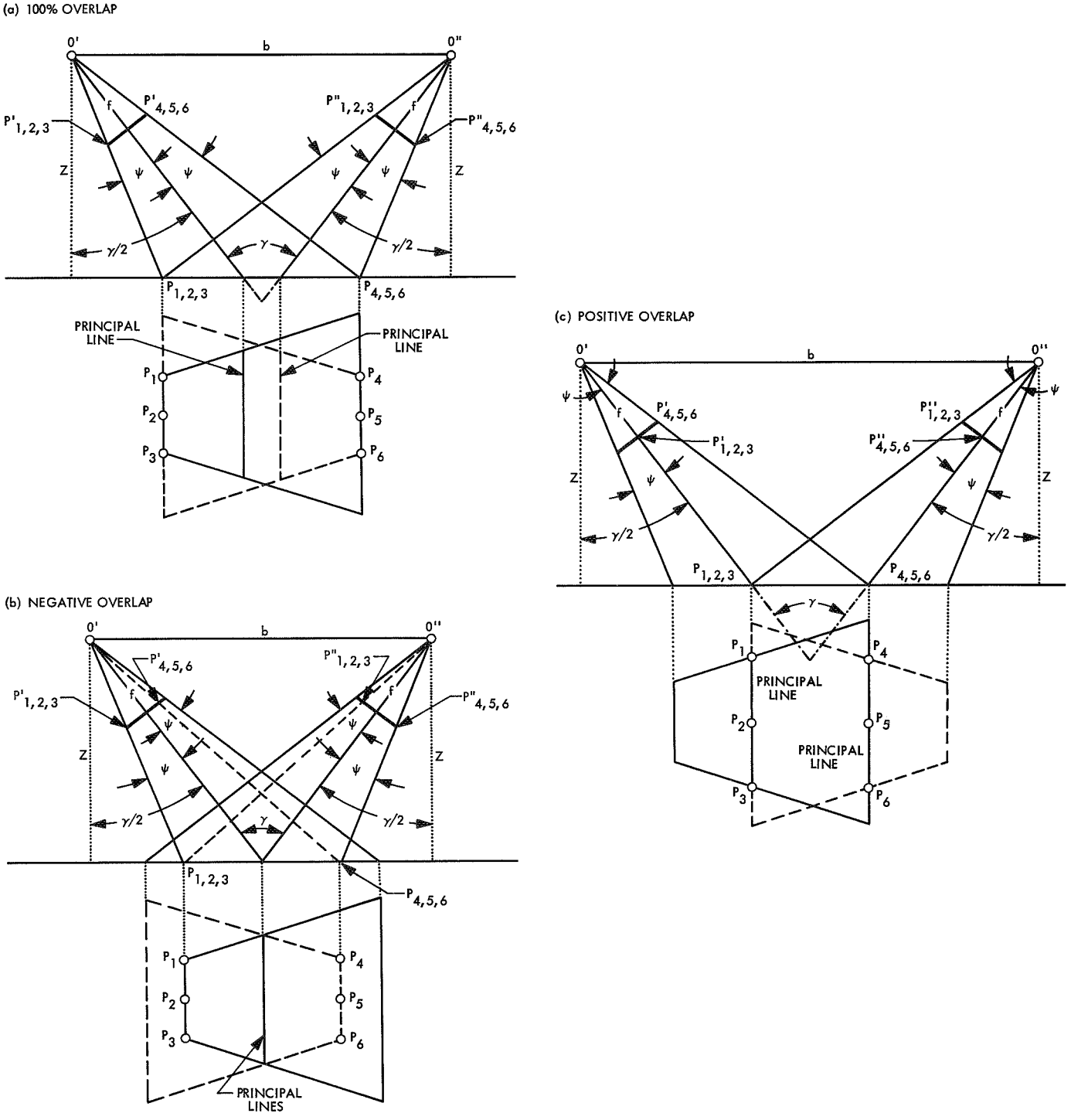

Fig. 2. Overlap: 100%, negative, and positive

camera coordinate system parallel with the ground system is computed from

$$\begin{bmatrix} \bar{x} \\ \bar{y} \\ \bar{z} \end{bmatrix} = \begin{bmatrix} \cos\frac{\gamma}{2} & 0 & \sin\frac{\gamma}{2} \\ 0 & 1 & 0 \\ -\sin\frac{\gamma}{2} & 0 & -\cos\frac{\gamma}{2} \end{bmatrix} \begin{bmatrix} x \\ y \\ -f \end{bmatrix} = \mathbf{R} \begin{bmatrix} x \\ y \\ -f \end{bmatrix} \tag{1}$$

Then, for a selected flight height Z, the X and Y ground coordinates are computed from

$$X = \bar{x}\frac{Z}{\bar{z}} \tag{3}$$

$$Y = \bar{y}\frac{Z}{\bar{z}} \tag{2}$$

To perform a successful relative orientation, image coordinates of six corresponding points on the left and right pictures must be known. As can be seen from Fig. 2, these points are different for each of the three basic overlap combinations. Their coordinates can be determined from modified Eqs. (1–3):

$$\bar{x} = X\frac{\bar{z}}{Z} \tag{2a}$$

$$\bar{y} = Y\frac{\bar{z}}{Z} \tag{3a}$$

where $\bar{z}$ is constant for each of the considered cross-sections.

Similarly,

$$\begin{bmatrix} x \\ y \\ z \end{bmatrix} = \mathbf{R}^{-1} \begin{bmatrix} \bar{x} \\ \bar{y} \\ \bar{z} \end{bmatrix} \tag{1a}$$

and since $\mathbf{R}$ is an orthogonal matrix

$$\begin{bmatrix} x \\ y \\ z \end{bmatrix} = \mathbf{R}^{T} \begin{bmatrix} \bar{x} \\ \bar{y} \\ \bar{z} \end{bmatrix} \tag{1b}$$

It is also evident that for all computed points, z must be equal to $-f$. This property can be used as a good computational check.

Furthermore, it is necessary to determine the stereophotogrammetric base for each of the three basic overlap combinations. Using Fig. 2, these relations are derived:

$$\text{HPO:}\quad b = Z\left[\tan\left(\frac{\gamma}{2} - \psi\right) + \tan\left(\frac{\gamma}{2} + \psi\right)\right] \tag{4}$$

$$\text{NO:}\quad b = 2Z\tan\frac{\gamma}{2} \tag{5}$$

$$\text{PO:}\quad b = Z\left[\tan\left(\frac{\gamma}{2}\right) + \tan\left(\frac{\gamma}{2} + \psi\right)\right] \tag{6}$$

These preliminary computations take care of the convergency–overlap problem; however, in an effort to represent a wide variety of image format–focal length combinations, the following parameters were chosen for investigation:

Format	12.5 mm: small vidicon (*Surveyor* or *Mariner* type)
	25 mm: Large vidicon (not yet available)
	70 mm: *Lunar Orbiter* type film processing
	200 mm: Large format film used in conventional photogrammetry (for comparison purposes only; its utilization in extraterrestrial photogrammetry is not presently feasible)
Focal length	25, 100, and 500 mm

These combinations represent a reliable realistic sample of convergent stereophotogrammetric cases that are applicable for extraterrestrial mapping purposes. They were subjected to the complex error analysis described in Refs. 1 and 2; the results obtained and conclusions reached are described in detail in the sections that follow.

III. Relative Orientation

Relative orientation based on the principle of collinearity has been described in detail in Refs. 1 and 2; however, when relative orientation is applied to convergent photography, certain additional conditions must be met.

A. Basic Approach

The procedure is shown schematically in Fig. 3; the symbols used are defined as follows:

O', O'' = left and right camera center of projection

X_0'', Y_0'', Z_0'' = base components in the left camera system

x', y', x'', y'' = observed image coordinates

z', z'' = left and right camera focal length

γ = angle of convergency

x''^*, y''^*, z''^* = image coordinates rotated from the right into the left camera system

$\mathbf{A}$ = orthogonal rotational matrix going from "ground" into "photo"

X_0, Y_0, Z_0 = model coordinates of an observed point in the left camera system

X_G, Y_G, Z_G = model coordinates of an observed point in the ground coordinate system

The basic idea is the same as in the normal parallel case. The left camera system remains fixed and all rotations (ω, ϕ, κ) and translations (Y_0'', Z_0'') are performed in the right camera system until all corresponding rays intersect at a proper elevation and without any model Y-parallaxes.

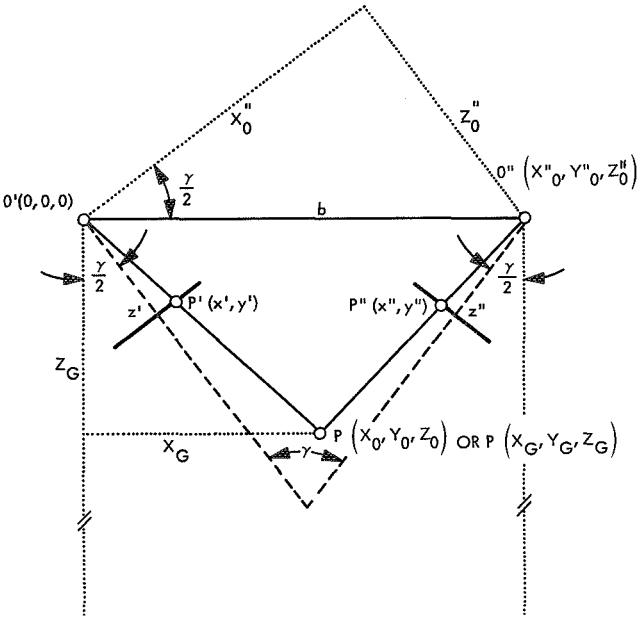

Fig. 3. Relative orientation applied to convergent photography

These five unknown parameters are determined by an iterative least-squares adjustment. The X-component of the base X_0'' is again deliberately chosen as equal to one, because, in relative orientation, scaling is of no interest; however, two more approximate starting values must be supplied: the Z-component of the base Z_0'' and rotation ϕ'':

$$Z_0'' = -\tan\frac{\gamma}{2}$$

$$\phi'' = \gamma$$

If the right camera is properly oriented with respect to the left camera, model coordinates of any measured point can be computed in the left camera system:

$$Z_0 = \frac{Z_0'' x''^* - z''^*}{x'^* - \frac{x'}{z'} z''^*} \tag{7}$$

where

$$\begin{bmatrix} x''^* \\ y''^* \\ z''^* \end{bmatrix} = \mathbf{A}^T \begin{bmatrix} x'' \\ y'' \\ z'' \end{bmatrix} = \mathbf{A}^T\mathbf{C} \tag{8}$$

and also

$$X_0 = \frac{x'}{z'} Z_0 \tag{9}$$

$$Y_0 = \frac{y'}{z'} Z_0 \tag{10}$$

Model coordinates X_0, Y_0, Z_0 would be of little practical use and, therefore, they must be further rotated into the ground coordinate system:

$$\begin{bmatrix} X_G \\ Y_G \\ Z_G \end{bmatrix} = \begin{bmatrix} \cos\frac{\gamma}{2} & 0 & \sin\frac{\gamma}{2} \\ 0 & 1 & 0 \\ -\sin\frac{\gamma}{2} & 0 & \cos\frac{\gamma}{2} \end{bmatrix} \begin{bmatrix} X_0 \\ Y_0 \\ Z_0 \end{bmatrix} = \mathbf{R} \begin{bmatrix} X_0 \\ Y_0 \\ Z_0 \end{bmatrix} \tag{11}$$

In conventional photogrammetry, error analysis of relative orientation is of little importance because least-squares adjustment of all model points into given ground control points gives sufficient statistical criteria. However, in extraterrestrial photogrammetry, it is vitally important because of an absolute lack of reliable ground control points.

The detailed mathematical derivation of this error analysis can be found in Refs. 1 and 2; therefore, only final results will be given here.

Standard errors of any computed model point can be determined from:

$$\mathbf{M}_0^2 = \begin{bmatrix} m_{X_0}^2 & m_{X_0Y_0} & m_{X_0Z_0} \\ m_{X_0Y_0} & m_{Y_0}^2 & m_{Y_0Z_0} \\ m_{X_0Z_0} & m_{Y_0Z_0} & m_{Z_0} \end{bmatrix} = \mu^2 \mathbf{SQS}^T \qquad (12)$$

where

$\mathbf{M}_0^2$ = variance–covariance matrix of a model point

μ = standard error of unit weight

$\mathbf{Q}$ = inverse weight matrix of the 14 or 11 parameters involved

$\mathbf{S}$ = coefficient matrix of observation equations

When two different cameras are used, these 14 parameters are involved in the error analysis:

ω, ϕ, κ = rotations of the right camera with respect to the left camera

Z_0'' = Z-component of the base

x_m', y_m', x_m'', y_m'' = measured left and right image coordinates

x_p', y_p', x_p'', y_p'' = left and right principal point eccentricity

z', z'' = left and right camera focal length

If the same camera is used for both exposures, certain simplifications are possible: it is evident that

$$z' = z'' = z, \qquad x_p' = x_p'' = x_p, \qquad y_p' = y_p'' = y_p$$

and the number of parameters is reduced to 11.

The reliability of this relative orientation error analysis is to a great extent dependent on the determination of the elements (co-factors) of the inverse weight matrix $\mathbf{Q}$.

A complete array of co-factors of the first four parameters (i.e., ω, ϕ, κ, and Z-base component Z_0'') can be obtained directly from the relative orientation least-squares adjustment, which definitely must be done.

However, the remaining co-factors, particularly the mixed terms, present a different problem. Theoretically, the observed image coordinates x', y', x'', y'' are correlated with the parameters mentioned earlier and, consequently, all mixed co-factors should be determined. But these correlations are based upon extremely complicated mathematical relations that make their complete computation prohibitively difficult and time consuming. Moreover, general analytical experience shows that the influence of such co-factors usually is very small. It was decided, therefore, to treat these co-factors as uncorrelated and to assign zero values to all these mixed terms. Thus, only the co-factors on the main diagonal are considered to be relevant.

However, it is absolutely necessary to reduce all co-factors to the same basic standard error of unit weight; otherwise, completely misleading and false results would be received.

The remaining parameters (i.e., principal point eccentricities x_p', y_p', x_p'', y_p'' and focal lengths z', z'') present still another problem. In this case, there can be no doubt that correlations between these parameters and those mentioned earlier can be neglected, which results in a simple determination of their corresponding co-factors along the main diagonal only. They may be correlated to some extent between themselves, depending upon the method of their original calibration, but this is not significant. These aspects are discussed in Sections V and VII of this report; however, for given purposes, they were assumed to be uncorrelated as well.

B. Consideration of Additional Error Influences

This was the original approach of analytical error analysis application to fictitious convergent photogrammetric stereopairs described in Section II. The results obtained showed a very interesting pattern, and, therefore, it was necessary to expand considerably the planned research activities by investigating new important fields of error influences.

This conclusion can be considered of fundamental importance. It was proven that the influence of errors of interior orientation parameters (i.e., focal length and principal point eccentricity) upon the accuracy of relative orientation is negligible and insignificant if these parameters are calibrated within a reasonable degree of accuracy.

On the other hand, the situation is completely changed and gains a new significance if the calibration of parameters is not correctly performed, is incomplete, or is not performed at all. This very often has been the case in technical practice, and experience has shown that inaccuracies incurred this way can become quite large.

In this case, the influence and propagation of these calibration errors tends to be strictly systematic, although their origin definitely is random. This can result in very unpleasant consequences. It is necessary, therefore, to treat these errors separately as systematic errors, rather than as random errors, if realistic and reliable conclusions are to be obtained.

This was done in an exhaustive manner; the results and conclusions are discussed in Section V. The results and conclusions shed new light on problems connected with interior orientation calibration that are described in Section VII. The following fictitious convergent stereomodels were used for this error analysis:

Small vidicon

$\gamma =$ 40 deg ($f = 25, 100, 500$ mm; $b/Z = 0.7$–1.0)

$\gamma =$ 80 deg ($f = 25, 100, 500$ mm; $b/Z = 1.7$–2.2)

$\gamma =$ 120 deg ($f = 25, 100, 500$ mm; $b/Z = 3.5$–5.1)

Large vidicon

$\gamma =$ 40 deg ($f = 25, 100, 500$ mm; $b/Z = 0.7$–1.4)

$\gamma =$ 80 deg ($f = 25, 100, 500$ mm; $b/Z = 1.7$–3.0)

$\gamma =$ 120 deg ($f = 25, 100, 500$ mm; $b/Z = 3.5$–14.8)

Lunar Orbiter

$\gamma =$ 40 deg ($f = 100, 500$ mm; $b/Z = 0.7$–1.2)

$\gamma =$ 80 deg ($f = 100, 500$ mm; $b/Z = 1.7$–2.5)

$\gamma =$ 120 deg ($f = 100, 500$ mm; $b/Z = 3.5$–7.0)

Large format

$\gamma =$ 40 deg ($f = 100, 500$ mm; $b/Z = 0.7$–2.5)

$\gamma =$ 80 deg ($f = 100, 500$ mm; $b/Z = 1.7$–12.3)

$\gamma =$ 120 deg ($f = 100, 500$ mm; $b/Z = 3.5$–4.7)

All these models were then computed for 100% overlap, negative overlap, and positive overlap, except in the case of large format ($\gamma = 120$ deg, $f = 100$ mm), where only negative overlap was possible. This also explains the relatively small range for the base-to-height ratio for this model as compared with the other models, particularly with the *Lunar Orbiter* type.

The success or failure of any error analysis is dependent upon the quality and reliability of the initial information; i.e., valid interpretations and conclusions can result only from properly collected and representative data.

It is believed that the statistical sample, represented by the aforementioned stereomodels, is fully reliable and realistic in this respect.

The flight height was deliberately chosen as equal to 1000 km, and only the base-to-height ratio was changed to obtain the desired overlap (see Section II). This was possible because all standard errors were computed in percentages of the spacecraft altitude, which enables a convenient application of this error analysis to any practical problem. In reality, the propagation of errors will not necessarily be linear with respect to altitude because of diminishing resolution, general image quality, etc. However, this influence can be overcome simply by proportionately increasing or decreasing image observation accuracy.

To simulate a correct propagation of errors for each of the contemplated convergent stereomodels, the procedure described in the paragraphs that follow was adopted.

It was desired that the standard observational error be tabulated in steps of 5 μm; therefore, image coordinates of each of the six points involved in relative orientation adjustment (see Section II) were changed on both images by 3.75 μm.

The ratio between these two values is equal to 0.75, which is approximately the ratio between the average and the standard error. This approach proved to be correct because all residual and standard errors resulting from the least-squares adjustment corresponded favorably to their original assumed values.

However, one more step is necessary to fully adapt the aforementioned relative orientation error analysis to convergent photogrammetric cases.

As shown in Fig. 3, Eqs. (7), (9), and (10) determine model coordinates in a system rotated by $\gamma/2$ with respect to the ground coordinate system, and, consequently, corresponding standard errors computed from Eq. (12) relate to the same inclined system.

These results, of course, are of little practical value and must be further transformed into the ground coordinate system to gain real significance.

Following the rules of error propagation for a function of dependent variables, this equation can be written:

$$\mathbf{M}_G^2 = \mathbf{R}\,\mathbf{M}_0^2\,\mathbf{R}^T \qquad (12a)$$

where

$\mathbf{M}_G^z$ = variance–covariance matrix of a model point transformed into the ground coordinate system

$\mathbf{R}$ = rotational matrix from Eq. (11)

$\mathbf{M}_0^z$ = variance–covariance matrix of an untransformed model point computed from Eq. (12)

C. Results

1. General discussion. Results of the error analyses are shown in Fig. 4 according to the pertinent stereomodels mentioned earlier (i.e., small vidicon, large vidicon, *Lunar Orbiter*, and large format).

The vertical scale represents observational standard errors of assumed TV images up to ± 25 μm and the horizontal scale shows the anticipated maximum standard height errors σ_Z/Z. The empirical limit (0.025%) used in conventional photogrammetry is marked by a dashed line.

The curves representing the propagation of errors are numbered according to respective parameter combinations (i.e., convergency–overlap–focal length and b/Z ratio combinations) that are described in a table in the upper part of each graph.

The information obtained from Fig. 4 would not be complete if it were not possible to know the difference between the maximum and minimum standard height errors. This supplemental information is given in Table 1. The average standard error can thus be expected to lie somewhere between these two extreme limits.

Table 1. Relative orientation: difference between maximum and minimum standard height errors

Stereomodel	Standard height error, %		
	FL[a] = 25 mm	FL = 100 mm	FL = 500 mm
Small vidicon	30	30	5
Large vidicon	25	45	5
Lunar Orbiter	—	20	40
Large format	—	15	30

[a]FL = focal length.

The resulting maximum standard height errors σ_Z/Z, although expressed in percentages of the flight height, should be considered as absolute errors (i.e., pertaining to two or more different relative orientations of the same model, or to relative orientations of two or more models).

If one relative orientation of one model only is considered, then resulting relative standard errors are somewhat smaller than those shown in Fig. 4. However, these errors have a very doubtful significance and, therefore, have not been analyzed for the purpose of this report.

Positional standard errors σ_X and σ_Y do not require a special analysis either as they are correlated with σ_Z and are usually smaller, or at least of the same order.

2. Interpretation of results. The manner in which Fig. 4 is composed enables the following convenient multiple interpretation to be made.

a. Determination of anticipated mapping accuracy. For known or assumed definite spacecraft system parameters and for known or assumed image accuracy, anticipated mapping accuracy can be determined.

Example: The spacecraft system parameters are defined by $\gamma = 80$ deg, 100% overlap, and $f = 100$ mm. (Because the camera is equipped with a small vidicon format, refer to Fig. 4a.) From the table in Fig. 4a, it can be determined that curve 3 is representative of this particular combination. Furthermore, it is expected that observational standard errors will be between ± 10 and ± 15 μm. Finding these values on the vertical scale and using curve 3, corresponding maximum standard height errors can be found on the horizontal scale as 0.1 and 0.16%. According to the data in Table 1, minimum errors differ from the maximum errors by 30% and, therefore, they can be expected to lie between 0.07 and 0.11%. The average mapping accuracy that can be reasonably expected can then be interpolated from these values.

b. Determination of parameters of a specific camera system. For required mapping accuracy and for known or assumed image accuracy, parameters of a specific camera system can be determined.

Example: *Lunar Orbiter*-type camera with $f = 500$ mm is used. Image accuracy is assumed to be ± 10 μm and the required mapping accuracy should not exceed 0.3%. The answer (i.e., the remaining spacecraft system parameters) can be found from Fig. 4a. It is apparent that curves 1–6 comply with the given requirements, which means that either $\gamma = 80$ deg (HPO, NO, PO) or $\gamma = 120$ deg (HPO, NO, PO) must be used, whereas $\gamma = 40$ deg

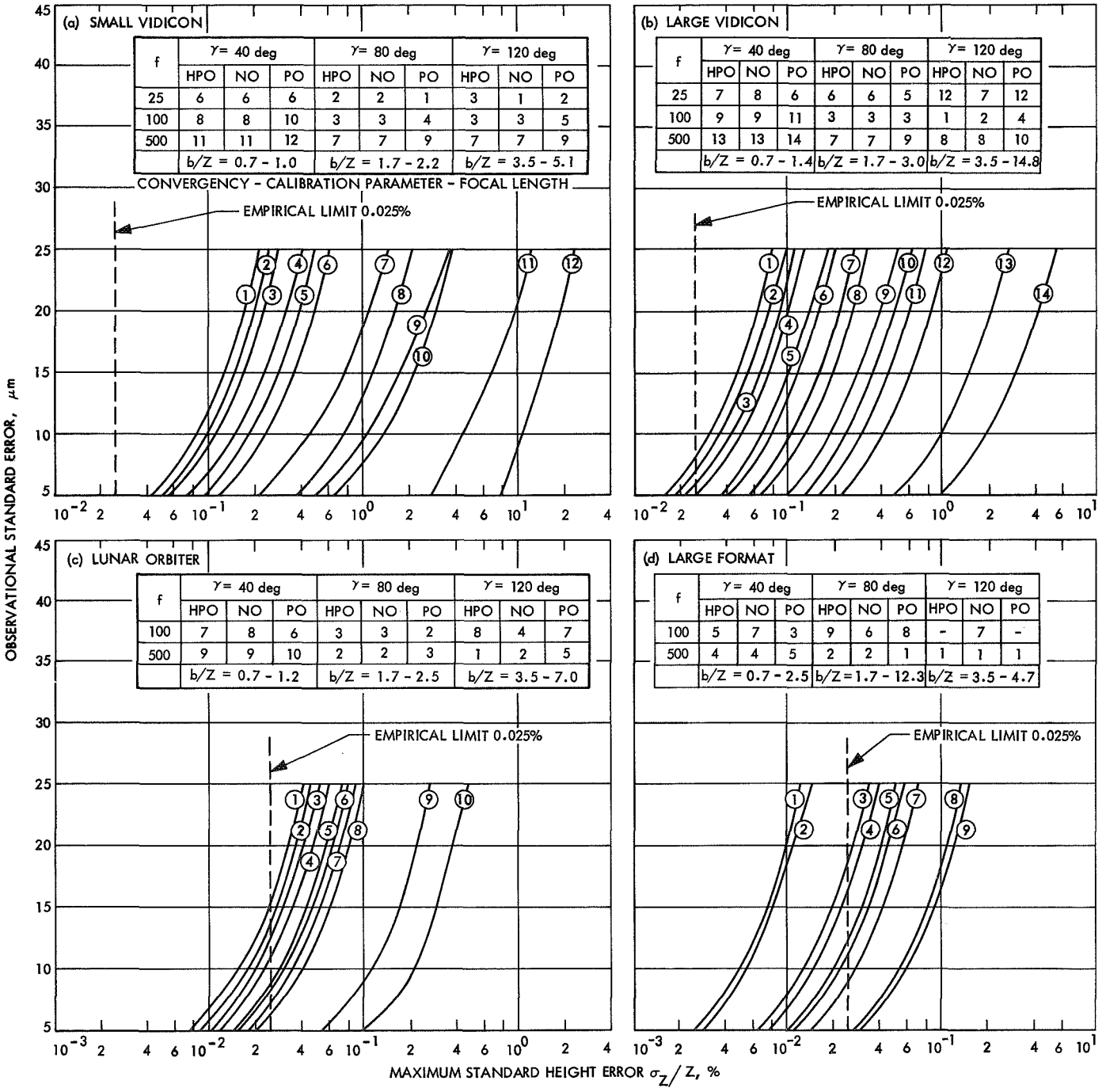

f	γ= 40 deg			γ= 80 deg			γ= 120 deg		
	HPO	NO	PO	HPO	NO	PO	HPO	NO	PO
25	6	6	6	2	2	1	3	1	2
100	8	8	10	3	3	4	3	3	5
500	11	11	12	7	7	9	7	7	9
	b/Z = 0.7 - 1.0			b/Z = 1.7 - 2.2			b/Z = 3.5 - 5.1		

f	γ= 40 deg			γ= 80 deg			γ= 120 deg		
	HPO	NO	PO	HPO	NO	PO	HPO	NO	PO
25	7	8	6	6	6	5	12	7	12
100	9	9	11	3	3	3	1	2	4
500	13	13	14	7	7	9	8	8	10
	b/Z = 0.7 - 1.4			b/Z = 1.7 - 3.0			b/Z = 3.5 - 14.8		

f	γ= 40 deg			γ= 80 deg			γ= 120 deg		
	HPO	NO	PO	HPO	NO	PO	HPO	NO	PO
100	7	8	6	3	3	2	8	4	7
500	9	9	10	2	2	3	1	2	5
	b/Z = 0.7 - 1.2			b/Z = 1.7 - 2.5			b/Z = 3.5 - 7.0		

f	γ= 40 deg			γ= 80 deg			γ= 120 deg		
	HPO	NO	PO	HPO	NO	PO	HPO	NO	PO
100	5	7	3	9	6	8	-	7	-
500	4	4	5	2	2	1	1	1	1
	b/Z = 0.7 - 2.5			b/Z = 1.7 - 12.3			b/Z = 3.5 - 4.7		

Fig. 4. Convergent photography relative orientation error analyses

(HPO, NO, PO) lie outside of the acceptable limits (this information can be extracted from the table shown in the upper part of the graph).

c. Determination of required observational image accuracy. For required mapping accuracy and for known or assumed definite camera system parameters, required observational image accuracy can be determined.

Example: The camera is equipped with a large vidicon format and the spacecraft system parameters are defined by $\gamma = 120$ deg and $f = 100$ mm. The required mapping accuracy should not exceed 0.05%. (In this case, it can readily be seen that curves 1, 2, and 4 in Fig. 4b must be used.) Using an approach similar to that described earlier, the necessary observational standard errors can be determined:

$$\pm 16.5\ \mu\text{m for } \gamma = 120 \text{ deg (HPO)}$$

$$\pm 14.0\ \mu\text{m for } \gamma = 120 \text{ deg (NO)}$$

$$\pm 10.0\ \mu\text{m for } \gamma = 120 \text{ deg (PO)}$$

This also was how the obtained data were analyzed.

3. Characteristics of convergent photography. Several conclusions can, therefore, be pointed out as characteristic of convergent photography.

a. Base-to-height ratio improvement. Base-to-height ratio is considerably improved as compared with the normal parallel case (Fig. 1).

External "forced" relative orientation (i.e., orientation based on supplied parameters) was the only solution for many normal parallel cases, as was shown in Refs. 1 and 2. This approach, however, is not necessary in convergent photography. This point is a very important and favorable conclusion.

The performed analysis has shown that the improved base-to-height ratio due to convergency guarantees better results for direct relative orientation than any practically obtainable data could achieve. Only for a few extreme cases might this method prove to be desirable (a detailed discussion of these aspects is given in Section IV).

b. Obtained accuracy improvement. It can responsibly be said that for the small vidicon the obtained accuracy can be improved at least 15 times compared with results described in Refs. 1 and 2, and, which is even more important, the accuracy is greater than that obtained from "external" relative orientation. For the large vidicon and the *Lunar Orbiter*-type photography, these differences were not determined, but they also can be expected to be of a considerable degree. The large format shows only a slight improvement, which was expected. These results are summarized in Table 2. "No data" entry means that this case was not computed, whereas "no solution" entry indicates that the system of normal equations was ill-conditioned and failed to converge. A more detailed comparison is given in Section IV.

Table 2. Accuracy comparison between convergent and normal stereomodels (for assumed observational error $\sigma = \pm 10\ \mu$m)

Stereomodel	Obtained accuracy, %		
	FL = 25 mm	FL = 100 mm	FL = 500 mm
Small vidicon			
Convergent	0.08–0.23	0.1–1.2	0.4–10.0
Normal	1.4–4.0	No solution	No solution
Normal ("external")	0.2–1.7	0.3–0.7	No data
Large format			
Convergent	—	0.013–0.06	0.005–0.02
Normal	—	0.02–0.3	No data
Normal ("external")	—	0.1–1.0	No data

It must be realized that this improvement is a function of convergency, image format, focal length, and changing image scale (i.e., overlap), and that this relation is rather complicated. These problems will be analyzed at length in the paragraphs dealing with individual image formats (stereomodels).

c. Design requirements. The performed error analysis clearly indicates that efforts to design a large format TV system will have to be undertaken, or some sort of *Lunar Orbiter*-type photography will have to be adapted if reliable and accurate mapping is desired as the primary objective of a planetary orbital or flyby mission.

The small vidicon, although its application to convergent photography shows a considerable accuracy improvement compared with normal photography, simply cannot achieve a fully satisfactory mapping capability, regardless of all technical precautions and of the highest care devoted to data collection and reduction.

d. Importance of measurement accuracy. The importance of highly accurate measurements for all image coordinates is clearly apparent from Fig. 4. The curves representing the law of propagation of errors are rather

flat and, therefore, the question of observational accuracy becomes a critical one.

This problem is closely related to the problem of image quality and of camera interior orientation calibration. Some of its aspects are described in Sections VI and VII; however, other research efforts on this subject would prove most rewarding.

D. Conclusions

Considering the representative stereomodels (i.e., according to image formats), the following conclusions can be drawn.

1. Small vidicon. The conclusions with respect to the small vidicon format are discussed in the paragraphs that follow.

a. Accuracy analysis according to individual focal lengths. A considerable improvement in mapping accuracy exists between $\gamma = 40$ and $\gamma = 80$ deg, whereas there is almost no difference between $\gamma = 80$ and $\gamma = 120$ deg. This conclusion pertains to all considered focal lengths.

b. Accuracy analysis according to individual convergencies. There is a noticeable decrease in accuracy for all convergent combinations with increased focal length. This seemingly defies the generally accepted parallax law of propagation of errors; however, it should be recollected that exactly the same phenomenon was encountered in normal parallel cases too (Refs. 1 and 2). This discrepancy was explained as being due to difficulties connected with the very narrow angle vidicon photography and evidently not even convergent combinations are able to completely eliminate this drawback.

c. Absolute mapping accuracy. Assuming an observational error $\sigma = \pm 10$ μm, the following combinations can be expected to result in a final mapping accuracy between 0.05 and 0.1%:

For $f = 25$ mm: $\gamma = 80$ deg (HPO, NO, PO) and $\gamma = 120$ deg (HPO, NO, PO)

For $f = 100$ mm: $\gamma = 80$ deg (HPO, NO) and $\gamma = 120$ deg (HPO, NO)

For $f = 500$ mm: none

All other combinations exceed the 0.1% limit and, therefore, are not accepted as sufficiently accurate.

These errors, of course, represent the maximum standard height errors; minimum or estimated average values may be obtained from Table 1.

d. General conclusions. Thus, as was mentioned earlier, the general conclusion for the small vidicon format appears not to be too favorable. Although there is a remarkable improvement on the order of magnitude between the normal and convergent cases, the absolute mapping accuracy still lies far to the right of the empirical limit of 0.025%, regardless of the precautions taken or the special arrangements made.

2. Large vidicon. The conclusions with respect to the large vidicon format are discussed in the paragraphs that follow.

a. Accuracy analysis according to individual focal lengths. The accuracy analysis according to individual lengths is as follows:

For $f = 25$ mm: slight improvement between $\gamma = 40$ and $\gamma = 80$ deg; considerable decrease between $\gamma = 80$ and $\gamma = 120$ deg

For $f = 100$ mm: considerable increase between $\gamma = 40$ and $\gamma = 80$ deg; almost no difference between $\gamma = 80$ and $\gamma = 120$ deg

For $f = 500$ mm: considerable increase between $\gamma = 40$ and $\gamma = 80$ deg; slight improvement between $\gamma = 80$ and $\gamma = 120$ deg

b. Accuracy analysis according to individual convergencies. The accuracy analysis according to individual convergencies is as follows:

For $\gamma = 40$ deg: gradual decrease with increased focal length

For $\gamma = 80$ deg: increase between $f = 25$ and $f = 100$ mm; decrease between $f = 100$ and $f = 500$ mm

For $\gamma = 120$ deg: considerable increase between $f = 25$ and $f = 100$ mm; considerable decrease between $f = 100$ and $f = 500$ mm

Thus, the parallax law discrepancy, so significant for the small vidicon format, is much less significant here. This can be viewed as a very favorable conclusion.

c. Absolute mapping accuracy. Assuming an observational error $\sigma = \pm 10$ μm, these combinations can be

expected to result in a final mapping accuracy between 0.03 and 0.05%:

For $f = 100$ mm: $\gamma = 80$ deg (HPO, NO, PO) and $\gamma = 120$ deg (HPO, NO, PO) and these between 0.05 and 0.1%:

For $f = 25$ mm: $\gamma = 40$ deg (HPO, NO, PO), $\gamma = 80$ deg (HPO, NO, PO), and $\gamma = 120$ deg (NO)

For $f = 500$ mm: $\gamma = 80$ deg (HPO, NO) and $\gamma = 120$ deg (HPO, NO)

All other combinations exceed these limits, some to a great degree.

Again, the difference between these maximum standard height errors and their minimum and estimated average values can be found in Table 1.

d. General conclusions. These results can be considered as very good. Although most of the curves still lie to the right of the empirical limit line used in conventional photogrammetry, they are much closer to it and a considerable accuracy improvement exists between the small and the large vidicon formats. Therefore, all efforts should be devoted to the problem of development and construction of a large vidicon format. Based on this error analysis, this seems to be one of the main obstacles to a reliable and accurate extraterrestrial orbital or flyby mapping system.

3. Lunar Orbiter. The conclusions with respect to the *Lunar Orbiter* format are discussed in the paragraphs that follow.

a. Accuracy analysis according to individual focal lengths. The accuracy analysis according to individual focal lengths is as follows:

For $f = 25$ mm: not feasible

For $f = 100$ mm: accuracy increase between $\gamma = 40$ and $\gamma = 80$ deg; decrease between $\gamma = 80$ and $\gamma = 120$ deg

For $f = 500$ mm: considerable improvement between $\gamma = 40$ and $\gamma = 80$ deg; practically no change between $\gamma = 80$ and $\gamma = 120$ deg

b. Accuracy analysis according to individual convergencies. The accuracy analysis according to individual convergencies is as follows:

For $\gamma = 40$ deg: considerable accuracy decrease with increased focal length

For $\gamma = 80$ deg: mapping accuracy is practically the same for any focal length selected

For $\gamma = 120$ deg: gradual improvement between $f = 100$ mm and $f = 500$ mm

Thus, the parallax discrepancy influence can be found in $\gamma = 40$ deg models only, whereas error propagation for all the other convergent combinations is much more like in conventional photogrammetry.

c. Absolute mapping accuracy. Assuming an observational error $\sigma = \pm 10$ μm, almost all combinations can be expected to result in a final mapping accuracy between 0.015 and 0.03%. These are the only few exceptions:

For $f = 100$ mm: $\gamma = 40$ deg (HPO, NO) and $\gamma = 120$ deg (HPO, PO) lie between 0.03 and 0.04%

For $f = 500$ mm: $\gamma = 40$ deg (HPO, NO, PO) lie between 0.1 and 0.2%, which, of course, is unacceptable

Similarly, as before, these values represent maximum standard height errors; the minimum and estimated average values can be determined from Table 1.

d. General conclusions. These results can be considered excellent. A great majority of the curves either cross the empirical limit line, or lie very close to it, which means that the obtained results are practically equivalent to those of conventional photogrammetry. Therefore, *Lunar Orbiter*-type photography should be applied whenever possible.

4. Large format. The conclusions with respect to the large format are discussed in the paragraphs that follow.

a. Accuracy analysis according to individual focal lengths. The accuracy analysis according to individual focal lengths is as follows:

For $f = 25$ mm: not feasible

For $f = 100$ mm/HPO: considerable decrease between $\gamma = 40$ and $\gamma = 80$ deg; $\gamma = 120$ deg is not feasible

For $f = 100$ mm/NO: practically no change between $\gamma = 40$ and $\gamma = 120$ deg

For $f = 100$ mm/PO: considerable decrease between $\gamma = 40$ and $\gamma = 80$ deg; $\gamma = 120$ deg is not feasible

For $f = 500$ mm: considerable increase between $\gamma = 40$ and $\gamma = 80$ deg; practically no change between $\gamma = 80$ and $\gamma = 120$ deg

It must be realized that large format combinations were investigated for comparison purposes only, because under the present state-of-the-art conditions, their utilization in extraterrestrial photogrammetry is out of the question. However, the results obtained are very interesting. It is evident that with the exception of very large focal lengths, convergent combinations have a detrimental influence upon the mapping accuracy and, therefore, should be avoided.

b. Accuracy analysis according to individual convergencies. The accuracy analysis according to individual convergencies is as follows:

For $\gamma = 40$ deg: practically the same accuracy for any selected focal length

For $\gamma = 80$ deg: considerable improvement between $f = 100$ and $f = 500$ mm

For $\gamma = 120$ deg: considerable improvement between f = 100 and f = 500 mm (NO only, of course)

Thus, as could only be expected, the parallax discrepancy is completely absent from any of these combinations.

c. Absolute mapping accuracy. Assuming an observational error $\sigma = \pm 10$ μm, almost all combinations can be expected to result in a final mapping accuracy between 0.005% and 0.03%. This is the only exception:

For $f = 100$ mm: $\gamma = 80$ deg (HPO, PO) is approximately 0.055%

And, again, the minimum and estimated average values of standard height errors can be found in Table 1.

d. General conclusions. These results reflect the optimum conditions of conventional photogrammetry and can thus be considered as perfect. They also again indirectly confirm the correctness of the theoretical error analysis derived in Refs. 1 and 2.

Compared with normal parallel cases (see Refs. 1 and 2) only a few and small differences can be found. As was mentioned earlier, application of convergent photography to large formats and normal focal lengths cannot be recommended. Narrow-angle photography brings a certain increase of mapping accuracy, but this improvement cannot make up for all the other difficulties connected with evaluation of convergent models (see Section II), and, therefore, convergent photography should not be attempted whenever large format cameras are available.

5. Summary of conclusions. The most significant and important conclusions concerning relative orientation may be summarized as follows:

(1) Unlike normal parallel cases, convergent photography can successfully and satisfactorily be utilized in an orbital or flyby mission.

(2) Compared with normal parallel cases, convergent stereomodels not only make a direct evaluation of a small vidicon format stereomodel possible, but also result in considerably improved mapping accuracy, which is a fundamental and significant conclusion.

It must be realized that the capabilities of a convergent small vidicon system still remain to some extent limited and, as a result of this, highly accurate and reliable mapping requirements cannot be expected to be fully satisfied by its application, particularly not when narrow-angle photography is considered, which, of course, is the most likely case in extraterrestrial photogrammetry.

(3) The large vidicon format system yields much better overall results in this respect and, therefore, all efforts should be made to assure its timely development and construction.

(4) The *Lunar Orbiter* format size is unquestionably the best in all respects and, therefore, should be used for orbital or flyby mapping missions whenever possible. Thus, the image format becomes a key factor as far as mapping accuracy is concerned.

IV. External Relative Orientation

A. Approach

As has been explained (see Refs. 1 and 2), direct relative orientation of a normal photogrammetric stereopair based on narrow-angle photography either cannot be performed at all, or resulting residual and standard errors are excessively large.

Therefore, instead of using observed image coordinates for a direct relative orientation, trajectory parameters are used for an external "forced" relative orientation. In this manner, model coordinates can always be computed and, knowing the standard errors of these parameters and

applying the derived error analysis, the final mapping accuracy can be determined as well.

As was shown in Section III, this approach is not necessary in convergent photography. The performed error analysis has shown that convergent models guarantee better results for direct relative orientation than any practically obtainable data for normal stereopairs could achieve. This conclusion is apparent from Table 2.

To complete the investigation, it was also necessary to compare the differences between the direct and external solutions for the assumed convergent stereomodels themselves.

Equations (12) and (12a) were applied to the pertinent models described in Section III and four different tests were computed for each of them. The corresponding parameter accuracy combinations, which closely approximate linear distributions in image observations, are shown in Table 3. Interior orientation calibration errors have a tendency to act as systematic errors and will be treated as such in the following section. To be consistent, therefore, it was necessary for the given purpose to consider them as nonexistent. This fact is clearly reflected in Table 3.

Determination of the elements (co-factors) of the inverse weight matrix is very simple because, in this particular case, all involved parameters can be treated as uncorrelated and, therefore, only elements on the main diagonal are required. These elements must, of course, unconditionally be reduced to the same basic standard error of unit weight.

Otherwise, exactly the same approach as for direct solution was used; i.e., whenever possible, every model was computed for 100% overlap, negative overlap, and positive overlap, and the resulting standard height errors were shown in percentages of the flight height.

Table 3. External relative orientation: combinations of parameter accuracy

Standard error parameters	Test			
	1	2	3	4
Rotation, rad	0.00001	0.0001	0.001	0.003
dZ_0 base component, % of base	0.02	0.1	0.2	0.5
Image coordinates, μm	5	10	15	20
Principal point,[a] μm	—	—	—	—
Focal distance,[a] μm	—	—	—	—

[a]Errors for these parameters are considered nonexistent for this purpose.

B. Results

1. General discussion. The results of the performed error analysis are shown in Fig. 5, according to the assumed stereomodels (i.e., small vidicon, large vidicon, *Lunar Orbiter*, and large format).

Similarly, as before, only maximum standard height errors were considered in these graphs; minimum and interpolated average values can be found in Table 4.

2. Interpretation of results. The vertical scale represents parameter accuracy combinations from Table 3, but, otherwise, the graphs can be interpreted in exactly the same multiple way as those in Fig. 4.

a. Determination of anticipated mapping accuracy. For known or assumed definite spacecraft system parameters and for their known or assumed accuracy combination from Table 3, anticipated mapping accuracy can be determined.

Table 4. External relative orientation: difference between maximum and minimum standard height errors

Stereomodel	Standard height error, %		
	FL = 25 mm	FL = 100 mm	FL = 500 mm
Small vidicon	50	20	10
Large vidicon	80	30	10
Lunar Orbiter	—	70	20
Large format	—	75	50

Example: The spacecraft system parameters are defined by $\gamma = 120$ deg, negative overlap, and $f = 25$ mm. (Because the camera is equipped with a small vidicon format, refer to Fig. 5a.) From the Fig. 5a table, it can be determined that curve 3 is representative of this particular combination. Furthermore, it is expected that standard errors of the parameters used for external relative orientation correspond to those of test 3 in Table 3. The expected

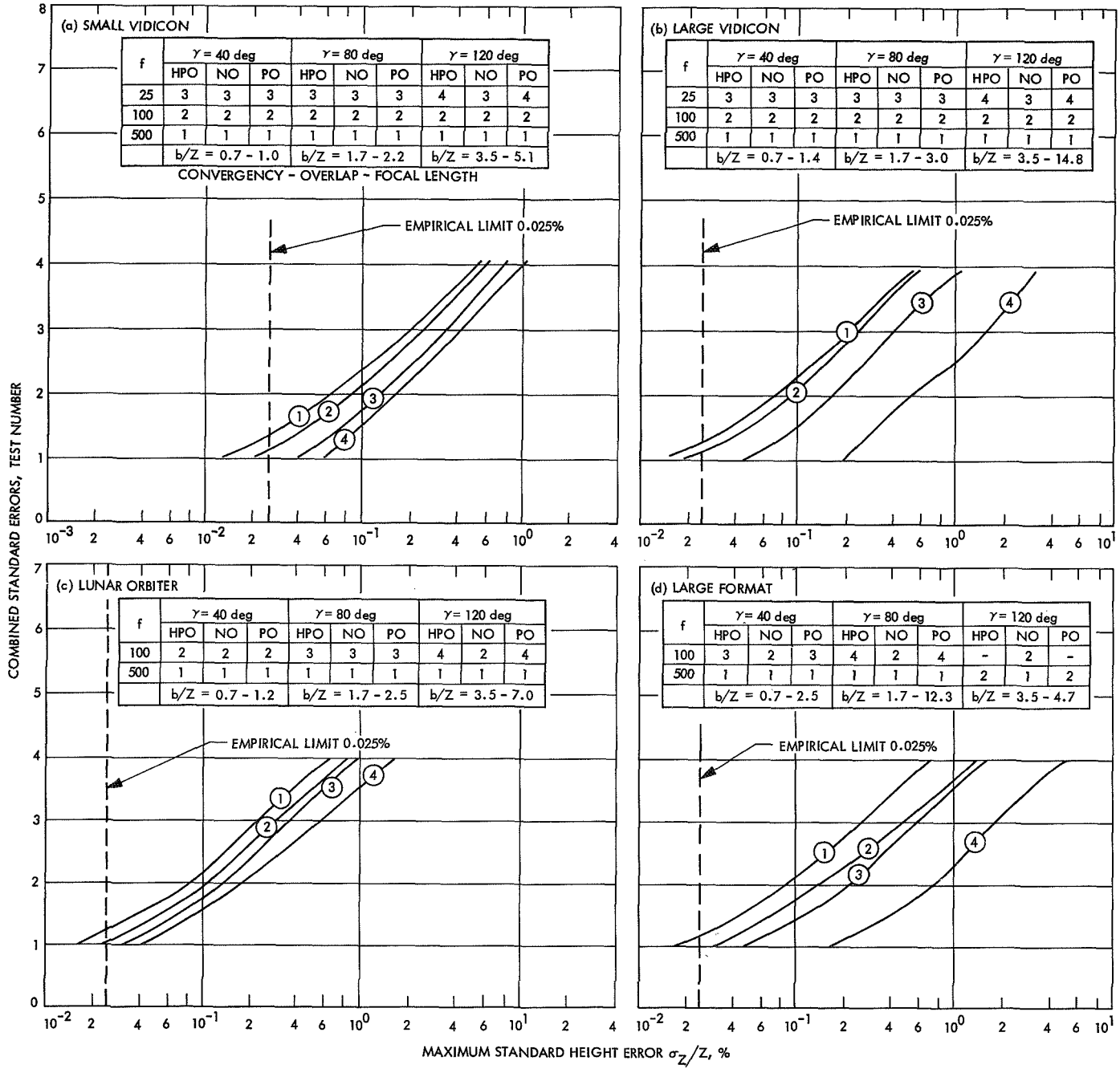

(a) SMALL VIDICON

f	γ = 40 deg			γ = 80 deg			γ = 120 deg		
	HPO	NO	PO	HPO	NO	PO	HPO	NO	PO
25	3	3	3	3	3	3	4	3	4
100	2	2	2	2	2	2	2	2	2
500	1	1	1	1	1	1	1	1	1
	b/Z = 0.7 - 1.0			b/Z = 1.7 - 2.2			b/Z = 3.5 - 5.1		

(b) LARGE VIDICON

f	γ = 40 deg			γ = 80 deg			γ = 120 deg		
	HPO	NO	PO	HPO	NO	PO	HPO	NO	PO
25	3	3	3	3	3	3	4	3	4
100	2	2	2	2	2	2	2	2	2
500	1	1	1	1	1	1	1	1	1
	b/Z = 0.7 - 1.4			b/Z = 1.7 - 3.0			b/Z = 3.5 - 14.8		

(c) LUNAR ORBITER

f	γ = 40 deg			γ = 80 deg			γ = 120 deg		
	HPO	NO	PO	HPO	NO	PO	HPO	NO	PO
100	2	2	2	3	3	3	4	2	4
500	1	1	1	1	1	1	1	1	1
	b/Z = 0.7 - 1.2			b/Z = 1.7 - 2.5			b/Z = 3.5 - 7.0		

(d) LARGE FORMAT

f	γ = 40 deg			γ = 80 deg			γ = 120 deg		
	HPO	NO	PO	HPO	NO	PO	HPO	NO	PO
100	3	2	3	4	2	4	-	2	-
500	1	1	1	1	1	1	2	1	2
	b/Z = 0.7 - 2.5			b/Z = 1.7 - 12.3			b/Z = 3.5 - 4.7		

Fig. 5. Convergent photography external relative orientation error analyses

mapping accuracy of 0.35% can then be found as an intersection of the horizontal line 3 and curve 3. This is, of course, the maximum standard height error; the minimum and average values can be estimated from Table 4 as 50 and 25% less, respectively.

b. Determination of a specific camera system. For required mapping accuracy and for known or assumed external parameter accuracy, a specific camera system can be determined.

Example: *Lunar Orbiter* size format with $f = 100$ mm is used. External parameter accuracy is assumed to correspond to results of test 2 in Table 3. The required mapping accuracy should be less than 0.15%. The remaining spacecraft system parameters (i.e., the convergency–overlap combinations) can be found from Fig. 5c. It is apparent that curves 1–3 comply with the given requirements and (referring to the attached table) this means that $\gamma = 40$ deg (HPO, NO, PO), $\gamma = 80$ deg (HPO, NO, PO), or $\gamma = 120$ deg (NO) must be used, whereas $\gamma = 120$ deg (HPO, PO) lie outside the acceptable limits.

c. Determination of required external parameter accuracy. For required mapping accuracy and for known or assumed definite camera system parameters, required external parameter accuracy can be determined.

Example: The camera is equipped with a large vidicon format and the spacecraft system is defined by $\gamma = 120$ deg and $f = 25$ mm. The required mapping accuracy should not exceed 0.2%. Referring to Fig. 5b, it can be seen immediately that curves 3 and 4 intersect the given limit. Using an approach similar to that described earlier, the necessary external parameter accuracy can be determined from Table 3:

Test (combination) 1 for $\gamma = 120$ deg (HPO, PO)

Test (combination) 2 for $\gamma = 120$ deg (NO)

C. Conclusions

Considering the representative stereomodels (i.e., according to image formats), the following conclusions can be drawn.

1. Small vidicon. The conclusions with respect to the small vidicon format are discussed in the paragraphs that follow.

a. Accuracy analysis according to individual focal lengths. The final mapping accuracy appears to be constant for any convergency–overlap combination.

b. Accuracy analysis according to individual convergencies. Mapping accuracy gradually improves with increased focal length; i.e., the parallax law discrepancy, which was so significant for the direct relative orientation solution, is not present here.

c. Absolute mapping accuracy. Assuming an external parameter accuracy combination equal to that of test 2 in Table 3, these spacecraft system combinations can be expected to result in a final mapping accuracy between 0.08 and 0.1%.

For $f = 25$ mm: none (they exceed this limit up to 0.17%)

For $f = 100$ mm and $f = 500$ mm: all convergency–overlap combinations

These are, of course, maximum standard height errors; their minimum and average values can be estimated from Table 4.

2. Large vidicon. The conclusions with respect to the large vidicon format are discussed in the paragraphs that follow.

a. Accuracy analysis according to individual focal lengths. The accuracy analysis according to individual focal lengths is as follows:

For $f = 25$ mm: mapping accuracy is constant, except for $\gamma = 120$ deg (HPO, PO) that show a sharp decrease

For $f = 100$ mm and $f = 500$ mm: constant

b. Accuracy analysis according to individual focal lengths. The conclusion is the same as that for the small vidicon.

c. Absolute mapping accuracy. Assuming test 2 qualifications, these spacecraft system combinations can be expected to result in a final mapping accuracy between 0.07 and 0.1%.

For $f = 25$ mm: none (they exceed this limit up to 0.55%)

For $f = 100$ mm and $f = 500$ mm: all convergency–overlap combinations

The difference between these maximum standard height errors and their minimum and interpolated average values can, again, be found in Table 4.

3. Lunar Orbiter. The conclusions with respect to the *Lunar Orbiter* format are discussed in the paragraphs that follow.

a. Accuracy analysis according to individual focal lengths. The accuracy analysis according to individual focal lengths is as follows:

For $f = 25$ mm: not feasible

For $f = 100$ mm: small decrease with increased convergency, only $\gamma = 120$ deg (NO) is the same as $\gamma = 40$ deg (HPO, NO, PO)

For $f = 500$ mm: constant

b. Accuracy analysis according to individual convergencies. Slight mapping accuracy improvement with increased focal length.

c. Absolute mapping accuracy. Assuming test 2 qualifications, these spacecraft system combinations can be expected to result in a final mapping accuracy between 0.08 and 0.11%.

For $f = 100$ mm: $\gamma = 40$ deg (HPO, NO, PO) and $\gamma = 120$ deg (NO), whereas $\gamma = 80$ deg (HPO, NO, PO) and $\gamma = 120$ deg (HPO, PO) exceed this limit up to 0.18%

For $f = 500$ mm: all convergency–overlap combinations

Similarly, as before, these values represent maximum standard height errors; the minimum and estimated average values can be determined from Table 4.

4. Large format. The conclusions with respect to the large format are discussed in the paragraphs that follow.

a. Accuracy analysis according to individual focal lengths. The accuracy analysis according to individual focal lengths is as follows:

For $f = 25$ mm: not feasible

For $f = 100$ mm/NO: constant

For $f = 100$ mm/HPO, PO: sharp decrease between $\gamma = 40$ and $\gamma = 80$ deg; $\gamma = 120$ deg is not feasible

For $f = 500$ mm: constant, except for $\gamma = 120$ deg (HPO, PO) that show a small decrease

b. Accuracy analysis according to individual convergencies. Mapping accuracy increases with increased focal length, in some cases considerably.

c. Absolute mapping accuracy. Assuming test 2 qualifications, these spacecraft system combinations can be expected to result in a final mapping accuracy between 0.08 and 0.15%:

For $f = 100$ mm: all negative overlap combinations fall within this limit, whereas all 100% and positive overlap combinations exceed it up to 0.7%

For $f = 500$ mm: all convergency–overlap combinations

Again, the minimum and average values of the standard height errors can be found in Table 4.

5. Summary of conclusions. The most important general conclusions concerning external relative orientation may be summarized as follows:

(1) Application of the external relative orientation method to narrow-angle convergent stereomodels totally eliminates the influence of the parallax law discrepancy; i.e., the mapping accuracy consistently increases with increased focal length.

(2) On the other hand, contrary to the direct relative orientation approach, the enlarged image format has a slightly detrimental effect upon the obtained mapping accuracy.

(3) Generally speaking, only a few curves in Fig. 5 cross the empirical limit line of 0.025% and they are also very flat. This means that extreme caution must be exercised whenever external relative orientation of convergent stereomodels is used; i.e., unless highly accurate input parameters are available, the final mapping accuracy diminishes very rapidly.

(4) The most important conclusion, however, results from the comparison of the convergent and exter-

nal convergent models with respect to their absolute accuracy.

To some extent, it is difficult to perform the comparison of convergent and external convergent models correctly because the previously assumed observational error $\sigma = \pm 10$ μm does not necessarily correspond to test 2 data in Table 3, so far as the other involved parameters are concerned.

As a matter of fact, based on a series of extensive experiments, it was found necessary to place this correspondence somewhere between tests 2 and 3. In this way, much more realistic and reliable results were obtained.

These results are shown schematically in Table 5. It can readily be seen that direct relative orientation of a convergent stereopair is not only possible, but also that it is better than its equivalent external solution, if the correct convergency–overlap combination is chosen. This accuracy increase is relatively small for small format and/or narrow-angle photography, but increases drastically when larger formats are used. This certainly can be considered as one of the most important and favorable conclusions of this report.

The only exception is represented by the small vidicon format ($f = 500$ mm), where the external solution is superior to the direct solution. Other exceptions would emerge if it were possible to obtain a parameter accuracy combination of about that of test 1 in Table 3. In this case, even small vidicon format ($f = 100$ mm) and large vidicon format ($f = 500$ mm) would give slightly better results for external solution than for direct solution. However considering the overall difficulties of TV photography and of extreterrestrial photogrammetric mapping, this can never be expected to happen.

This fact, however, only underlines the problems connected with small vidicon mapping that were described in detail in the previous section, and, at the same time, emphasizes the necessity to develop and build a large vidicon TV camera system.

Table 5. Accuracy comparison between convergent and external convergent stereomodels (for assumed observational error $\sigma = \pm 10$ μm)

Stereomodel	Obtained accuracy, %		
	FL = 25 mm	FL = 100 mm	FL = 500 mm
Small vidicon			
Convergent	0.08–0.23	0.1–1.2	0.4–10.0
External convergent	0.2–0.3	0.15	0.12
Large vidicon			
Convergent	0.07–0.4	0.03–0.3	0.1–2.0
External convergent	0.25–1.0	0.15	0.13
Lunar Orbiter			
Convergent	—	0.017–0.04	0.015–0.2
External convergent	—	0.18–0.3	0.14
Large format			
Convergent	—	0.013–0.06	0.005–0.02
External convergent	—	0.25–1.2	0.15–0.25

V. Systematic Calibration Errors

As was mentioned in previous sections, one of the very important conclusions of this study is that interior orientation errors resulting from calibration of the camera system tend to be strictly systematic, although their origin definitely is random.

The parameters involved are the focal length and the principal point eccentricity; i.e., the x and y difference between the geometrical image center defined by the reseau grid and the intersection point of the optical axis with the image plane (see Fig. 11).

It was also found that the influence of these parameters upon the final mapping accuracy can be neglected if calibration is correctly performed and the residual errors are kept within reasonable limits.

If this is not done, however, then the situation may be changed very rapidly. Experience has shown that calibration inaccuracies can become quite large (*Surveyor* photography is a good example in this respect), in which case their systematic influence can produce considerably distorted results.

A. Approach

Therefore, it was decided to treat these systematic errors in a separate series of investigations with the intent to define their propagation characteristics. This research was performed; results and conclusions are discussed in this section.

The fictitious convergent stereomodels described in previous sections were used for this error analysis.

Similarly, as with the relative and external relative orientation error analyses, these models were considered

for 100% overlap, negative overlap, and positive overlap, and the resulting average errors were computed from all these combinations.

In the interest of a realistic simulation of the desired systematic error propagation for each of the assumed convergent stereomodels, the procedure described in the following paragraphs was used.

The analytical approach itself was quite simple. No special error analysis was required; all that was necessary was to compute the relative orientation according to Eqs. (7–11) for different assumed calibration errors. The computed model coordinates, compared with their exact values, then explicitly determine the real absolute mapping accuracy that can be expected.

It was desired that the real absolute calibration error be tabulated in steps of 50 μm, which is different from previous computations where standard errors were used. Thus, the calibration parameters involved (i.e., focal length and principal point eccentricity) were directly changed without the necessity of converting assumed standard errors to their corresponding average values.

B. Results and Conclusions

1. Height mapping accuracy. Results of the error analysis that pertain to the height (Z-coordinate) mapping accuracy are shown in Fig. 6. The vertical scale represents real absolute calibration errors up to 500 μm, and the horizontal scale shows the corresponding average absolute height error $\sigma_{Z/Z}$, which is expressed in percentages of the flight height. The empirical limit (0.025%) used in conventional photogrammetry is again marked (curve 0 means that results are so good that they do not even show on the graph).

The curves representing the propagation of errors are numbered according to respective camera system combinations (i.e., convergency calibration parameters–focal length–σ/Z ratio combinations that are shown in an attached table).

Abbreviations used for the pertinent calibration parameters are *FD* (focal length), *PP* (principal point eccentricity), and *FD* + *PP* (combined influence of both of these parameters).

a. General discussion. In virtually all cases, the average absolute height errors $\sigma_{Z/Z}$ were computed from compact and evenly distributed values, which make the determination of their extreme values unnecessary. The few exceptions, some of them quite large, are shown in Table 6; the numbers indicate how many times the maximum error is larger and the minimum error smaller, respectively, than the anticipated average error. The minimum extremes are welcome, of course, but those camera system configurations with maximum influences should be treated with utmost caution.

Table 6. Systematic calibration errors: extreme values of influence

Focal length, mm	Stereomodel[a]							
	SV	LV	LO	LF	SV	LV	LO	LF
	Negative overlap				Positive overlap			
25	−4	−10	—	—	3	0	—	—
100	0	−3	−7	−10	10	5	0	0
500	0	0	−3	−4	50	40	10	3

[a] SV = small vidicon; LV = large vidicon; LO = Lunar Orbiter; LF = large format.

b. Interpretation of results. The data shown in Fig. 6 are subject to the following convenient multiple interpretation.

Determination of anticipated systematic influence. For known or assumed definite spacecraft system configurations and for known or assumed interior orientation calibration errors, anticipated systematic influence $\sigma_{Z/Z}$ can be determined:

Example: The spacecraft system parameters are defined by small vidicon, $\gamma = 80$ deg and $f = 100$ mm. Principal point eccentricity is accurately known, but focal length was not correctly calibrated, and its average error is expected to reach a value of up to ± 100 μm. From the table in Fig. 6a, it can be seen that curve 3 is representative of this case and, therefore, a negligible systematic influence of only 0.0012% can be expected. However, Table 6 must nevertheless be consulted for eventual extreme values. For this particular model, this means that 100% and negative overlap are unaffected, but positive overlap can have a few extreme points with a maximum error of up to 0.012%.

Determination of parameters of a specific spacecraft system. For a maximum tolerable systematic error and for known or assumed interior orientation calibration errors, parameters of a specific spacecraft system can be determined.

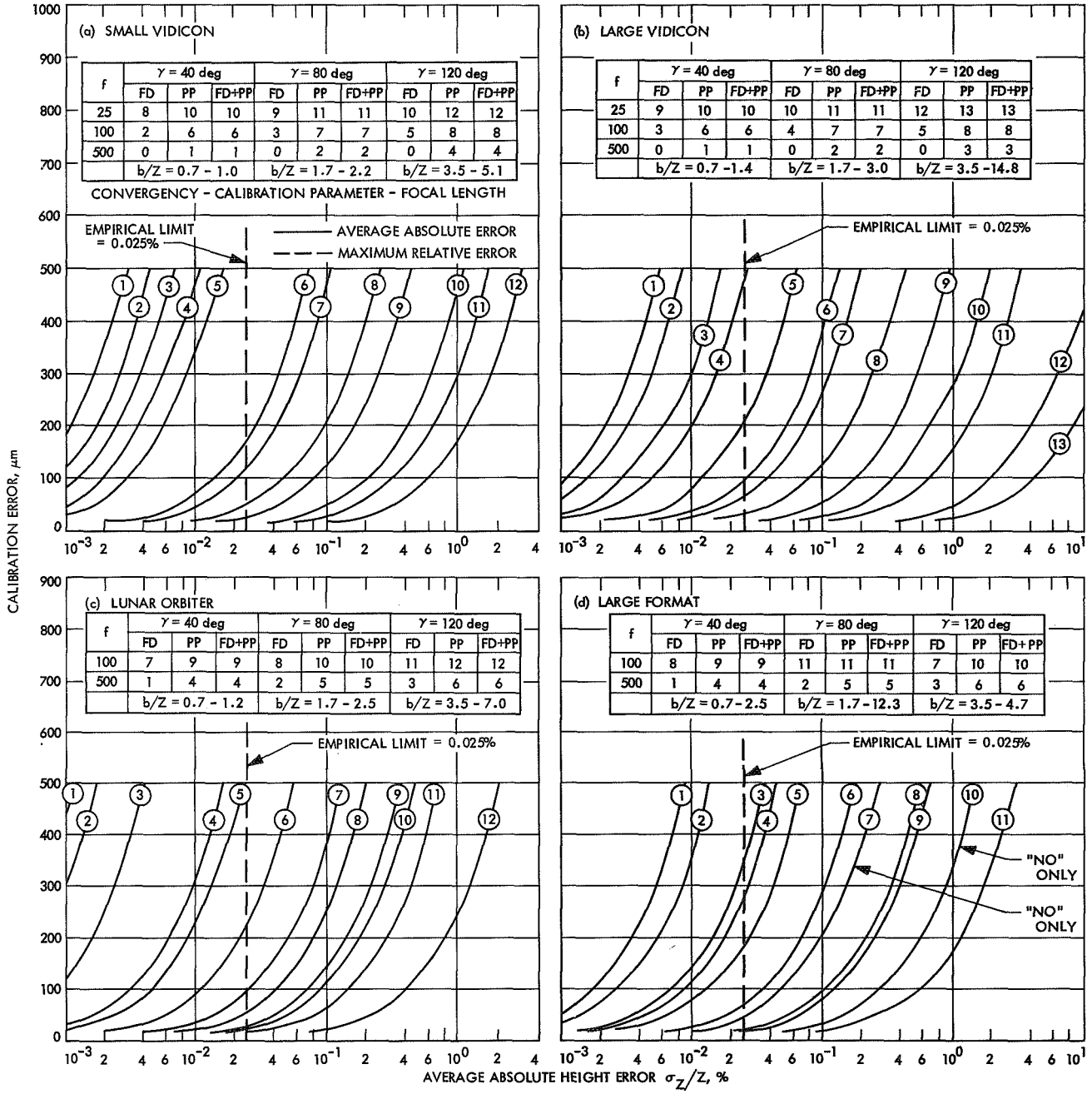

f	γ = 40 deg			γ = 80 deg			γ = 120 deg		
	FD	PP	FD+PP	FD	PP	FD+PP	FD	PP	FD+PP
25	8	10	10	9	11	11	10	12	12
100	2	6	6	3	7	7	5	8	8
500	0	1	1	0	2	2	0	4	4
	b/Z = 0.7 - 1.0			b/Z = 1.7 - 2.2			b/Z = 3.5 - 5.1		

f	γ = 40 deg			γ = 80 deg			γ = 120 deg		
	FD	PP	FD+PP	FD	PP	FD+PP	FD	PP	FD+PP
25	9	10	10	10	11	11	12	13	13
100	3	6	6	4	7	7	5	8	8
500	0	1	1	0	2	2	0	3	3
	b/Z = 0.7 -1.4			b/Z = 1.7 - 3.0			b/Z = 3.5 -14.8		

f	γ = 40 deg			γ = 80 deg			γ = 120 deg		
	FD	PP	FD+PP	FD	PP	FD+PP	FD	PP	FD+PP
100	7	9	9	8	10	10	11	12	12
500	1	4	4	2	5	5	3	6	6
	b/Z = 0.7 - 1.2			b/Z = 1.7 - 2.5			b/Z = 3.5 - 7.0		

f	γ = 40 deg			γ = 80 deg			γ = 120 deg		
	FD	PP	FD+PP	FD	PP	FD+PP	FD	PP	FD+PP
100	8	9	9	11	11	11	7	10	10
500	1	4	4	2	5	5	3	6	6
	b/Z = 0.7 - 2.5			b/Z = 1.7 - 12.3			b/Z = 3.5 - 4.7		

Fig. 6. Convergent photography systematic calibration errors: Z-coordinates

Example: *Lunar Orbiter*-format size with $f = 100$ mm is used. Focal length is perfectly calibrated, but principal point eccentricity is not known and can be assumed to reach a value of up to ± 50 μm. The resulting systematic influence should be kept below 0.05%. Figure 6c shows that curves 1–10 comply with these requirements, which, according to the attached table, means that a convergency of $\gamma = 40$ or $\gamma = 80$ deg must be used. Table 6 shows no extreme values for positive overlap, and only a considerable minimum influence for negative overlap, which is very favorable.

Definition of required maximum interior orientation calibration criteria. For maximum tolerable systematic error influence and for known or assumed spacecraft system parameters, required maximum interior orientation calibration criteria can be defined.

Example: The camera is equipped with a large vidicon format and the spacecraft system parameters are defined by $\gamma = 120$ deg and $f = 100$ mm. The maximum systematic error influence should not exceed 0.05%. From the table in Fig. 6b, it can readily be seen that curves 5 and 8 must be used. Using an approach similar to that used earlier, these calibration limits can be determined:

± 400 μm for focal length

± 60 μm for principal point eccentricity

To obtain a complete picture, one more problem must be realized. The systematic error influences discussed so far were of strictly absolute nature; however, whenever systematic errors occur, the importance of their relative differences becomes very critical.

It was decided, therefore, to determine, in addition to average absolute height errors $\sigma_{Z/Z}$ shown in Fig. 6, maximum relative height errors $\rho_{Z/Z}$ (i.e., relative height differences between two extreme model points).

Their values for any of the assumed stereomodels can be simply computed from these relations:

For focal length: $\max \rho_{Z/Z} = 0$

For principal point eccentricity: $\max \rho_{Z/Z} = 2\,\sigma_{Z/Z}$

For combined influence: $\max \rho_{Z/Z} = 2\,\sigma_{Z/Z}$

This means that all accuracy criteria derived from Fig. 6 should be correspondingly reduced whenever principal point eccentricity is involved and systematic relative differences are considered.

c. Conclusions. The analysis of systematic influences of interior orientation calibration errors (i.e., of focal length and principal point inaccuracies) upon the mapping accuracy of convergent stereomodels resulted in these important general conclusions:

(1) The influence drastically diminishes with increased focal length (for any convergency–image format combination).

(2) The influence considerably increases when larger image format is used (for any convergency–focal length combination).

(3) The influence rapidly increases with increased convergency (for any image–focal length combination).

(4) Principal point eccentricity has a much stronger influence than has focal length, which is reflected not only by their respective absolute errors, but also by the fact that the combined influence of both these parameters is practically equal to that of principal point eccentricity alone.

(5) Conclusions (1) and (2) taken together mean that influence is a function of the camera field of view.

Thus, in most of these cases, the systematic error propagation trend runs contrary to the random error trend described in earlier sections. This, of course, is unfavorable, but, fortunately, the magnitude of this systematic influence can usually be kept below the random level.

On the other hand, conclusions (1), (2), and (3) are extremely favorable from the calibration procedure standpoint and together can be considered one of the most significant contributions of this study.

It is apparent that calibration requirements can be kept very low, or in some cases even completely eliminated, if small image formats and/or large focal lengths are used. This is very fortunate, because, as is explained in Section VII, interior orientation calibration of such systems can become very difficult or even impossible.

However, when large image formats and/or small focal lengths (i.e., large fields of view) are used, these systematic influences can become very critical, particularly for increased convergencies. But, in these cases, accurate interior orientation calibrations should not be connected with any extraordinary difficulties.

Therefore, no matter what the combination or configuration, it is absolutely necessary to consult its respective systematic error propagation before any calibration is performed, or before any conclusions concerning the final mapping accuracy are made.

Conclusion (4) is then closely correlated with the other conclusions mentioned earlier. It has been a generally accepted practice in photogrammetry that focal length only was calibrated, usually with a high degree of accuracy, whereas principal point eccentricity was widely neglected. It can clearly be seen now that at least the same attention must be paid to the latter parameter as to the former if major systematic model distortions are to be avoided.

2. *X- and Y-error propagation.* As is explained in Sections III and IV, positional error analysis is not necessary when random errors only are involved. However, this assumption does not hold true for systematic errors. In this case, the X- and Y-error propagation is completely independent and can differ considerably from the height (Z-direction) mapping accuracy. It was decided, therefore, to treat these cases in a separate series of investigations. The results of this effort are shown in Figs. 7 and 8.

a. General discussion. The stereomodels and approach used for the height error analysis were used here; however, there are some minor changes and deviations that should be pointed out.

It would be very impractical to determine all absolute positional errors in percentages of their corresponding X or Y coordinates, and, instead, absolute positional errors were computed in relation to the same flight height (i.e., as $\sigma_{X/Z}$ and $\sigma_{Y/Z}$).

To save expensive computer time, systematic influence upon positional accuracy was computed for 100% overlap only. Thus, the obtained results reasonably well represent the average absolute positional errors, but it was not possible to determine any eventual extreme values as was done in Table 6 for the height accuracy. However, the eventual extreme values can be expected to be of about the same order and for the same stereomodels as shown in Table 6.

On the other hand, it was necessary to show the maximum relative positional errors by separate dashed curves in Figs. 7 and 8 because, with a few exceptions only, they do not follow the same consistent pattern as the height errors. If the dashed curve is identical with one of the solid curves, then this identity is indicated in the attached table by three parallel lines (e.g., $\equiv 9$).

b. Interpretation of results. This, of course, complicates the graphs, but a simple example will satisfactorily clarify them.

Example: The spacecraft system parameters are defined by small vidicon, $\gamma = 120$ deg and $f = 100$ mm. Focal length is accurately known, but principal point eccentricity was not calibrated and is expected to be equal to ± 200 μm.

The X-direction influence will be investigated first (see Fig. 7a). As the explanatory table shows, the average absolute error is represented by curve 11 (solid line) and the maximum relative error by curve 1′ (dashed line). It can clearly be seen that the relative influence is absolutely negligible, whereas the absolute error $\sigma_{X/Z} = 0.8\%$ is quite large. This, of course, makes any mapping results based on this particular stereomodel unacceptable, unless correct principal point calibration is performed.

An identical procedure is used for the Y-direction analysis. Curve 7′ in Fig. 8a defines an error of 0.16%, which cannot be neglected, and curve 11 defines an error of 0.4%. Therefore, the conclusion noted earlier can be repeated.

c. Conclusions. A similar error analysis can be derived for any other eventual parameter combination. Using Figs. 7 and 8, this was done, and these general conclusions become apparent for systematic positional errors:

(1) Error propagation considerably decreases with increased focal length (for any convergency–image format combination). The only exception is represented by the large format, which shows a few anomalies in the X-coordinate accuracy.

(2) The influence of focal length gradually increases when larger format is used, but is practically constant for principal point eccentricity and for the combined influence of both these parameters (with the exception of a few large format anomalies, this conclusion pertains to any convergency–focal length combination).

(3) The influence of systematic calibration errors slowly increases with increased convergency (for any image format–focal length combination).

(4) Principal point has a much stronger influence than focal length.

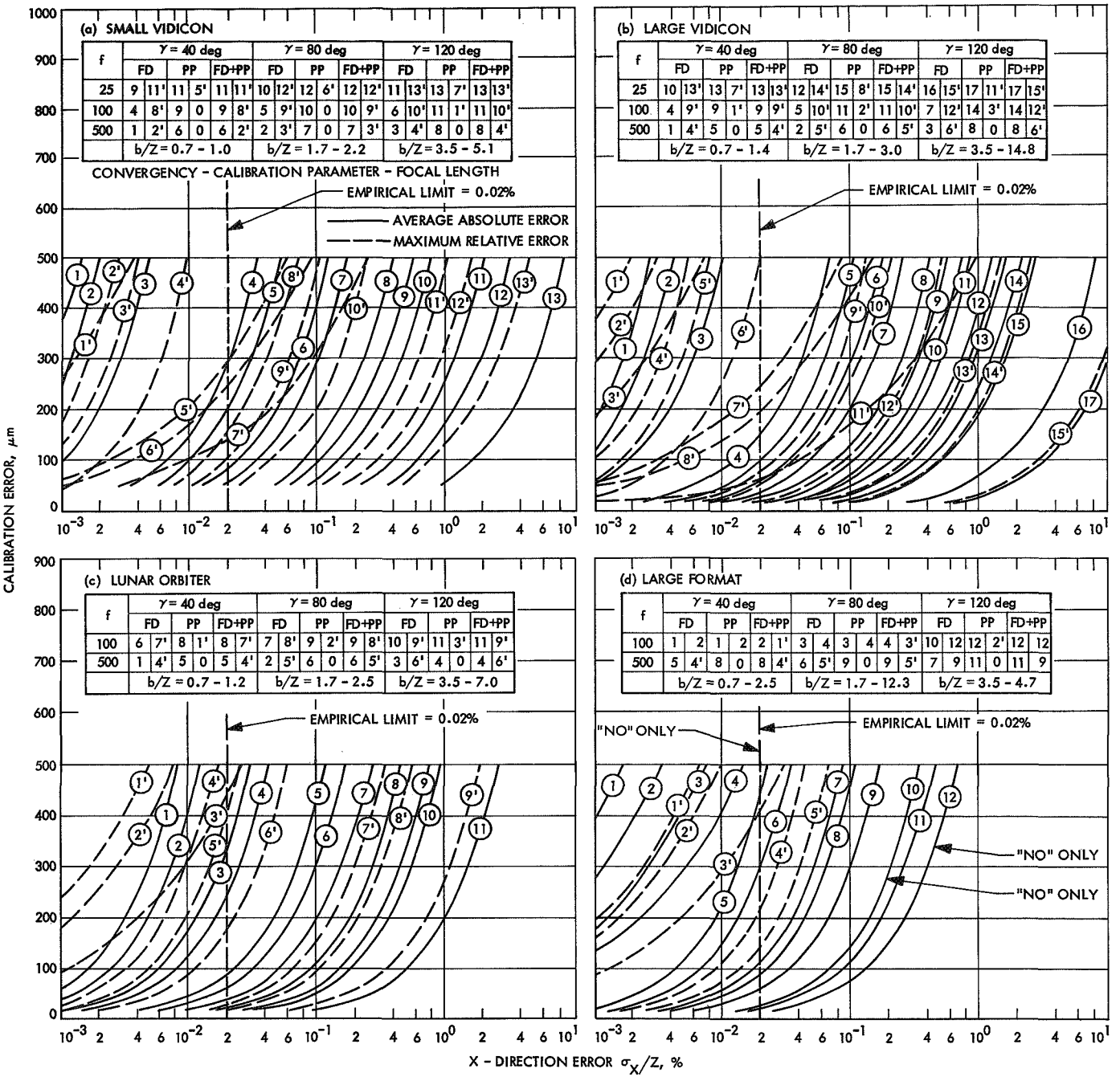

Fig. 7. Convergent photography systematic calibration errors: X-coordinates

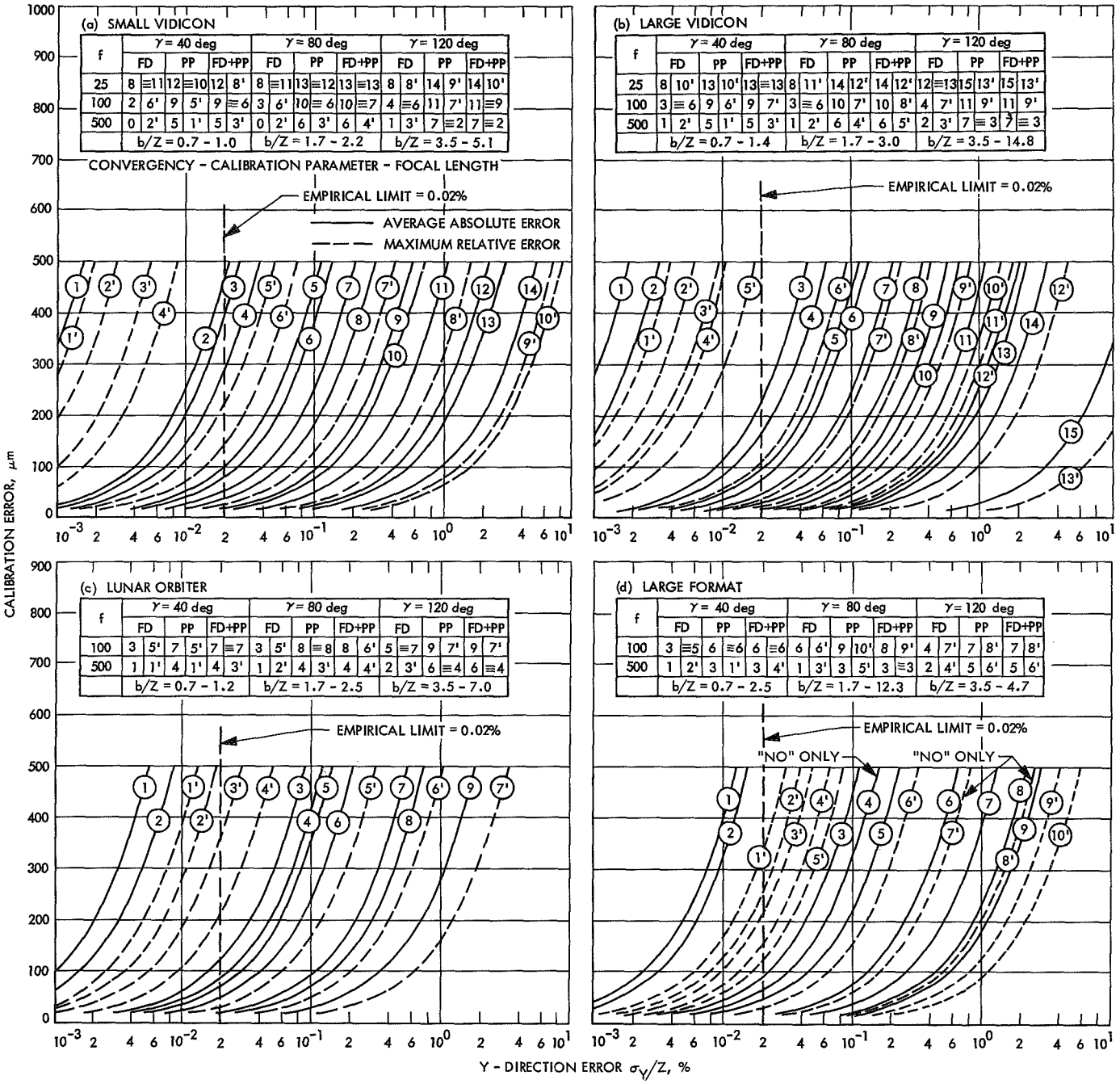

Fig. 8. Convergent photography systematic calibration errors: Y-coordinates

It can thus be seen that height and positional influences have basically the same trend, but their absolute magnitudes, and particularly their relative values, can differ considerably. This fact only confirms the necessity of their separate investigations.

3. General conclusions. The most significant conclusions concerning systematic calibration errors may be summarized as follows:

It is necessary to treat the interior orientation calibration errors (i.e., focal length and principal point eccentricity) as separate systematic errors, although their origin is random. Their influence on height and positional accuracy is different, and spreads from insignificant to unacceptable values. The desired graphs can conveniently be used for both error analysis and for determination of accuracy criteria of a specific spacecraft system; this should always be done.

VI. Image Quality

A. Approach

In an effort to make the investigations and their conclusions more relevant, a series of supplementary analog tests was performed. Whereas the preceding sections deal exclusively with theoretical problems of error analysis applied to convergent photogrammetry, this section and Section VII discuss the practical problems of image quality and interior orientation calibration, respectively.

The importance of highly accurate image measurements has been clearly shown. As can be seen from Figs. 4 and 5, the curves representing the law of error propagation are relatively flat (i.e., slope $\leqslant 1$), which means that the final mapping accuracy rapidly decreases with increased observational errors.

A great deal of progress has been made in this respect by the use of digital image processing techniques (Ref. 6); however, the absolute magnitude of the detrimental effect of TV scanning upon the image quality has not as yet been fully determined.

Therefore, the objective of the image quality tests was to find answers to these questions, particularly to those of image resolution and reseau mark quality.

In the context of this discussion, resolution is defined as ability of the camera system to distinguish fine image details. Resolution is not uniform and must be considered separately for different directions.

The vertical resolution, measured perpendicularly to the scan lines, is mainly affected by the scanning geometry. The horizontal resolution, measured in a direction parallel with the scan lines, is mainly influenced by system noise, the transmission channel, and the finite aperture of the scanning beam, and is usually better than the vertical resolution. Because of other system aberrations, resolution also decreases radially outward from the optical axis.

The theoretical and mathematical aspects of this problem have been described in detail (Ref. 7). Consequently, it is not necessary to repeat them in this report and full attention will be given to practical results.

The analog test itself was based on a test grid, which was set up on a smooth, flat wall. Using a Zeiss SMK-120 stereometric camera (image format 80×100 mm, focal length = 60 mm) a series of stereo pictures of this grid were taken. These pictures were then measured on a Mann monocomparator, which enabled determination of their observational and absolute orientation accuracy.

In the next step, the same pictures were converted to simulated TV photographs using a video film converter. Two different TV scan line widths (1000- and 600-line modes) were applied, and the signal-to-noise ratio was maintained at about 20:1, which characterizes very good pictures. The procedure was then repeated, and the comparison of the obtained results revealed interesting facts about TV image quality.

The test grid (Fig. 9) consisted of 25 points that were marked by special alignment targets (Fig. 10). These targets, which are produced by Keuffel & Esser Co., can conveniently be used for any image scale. The size of the grid is 2.6×2.6 m, which, at the chosen image scale, corresponds approximately to an image format of 35×35 mm (the SMK-120 camera was approximately 4.5 m away from the grid).

To obtain accurate and reliable results, the coordinates of the test grid had to be perfectly known. The method of trilateration was designed for this purpose.

All horizontal, vertical, and diagonal distances between the grid points were measured with a calibrated steel

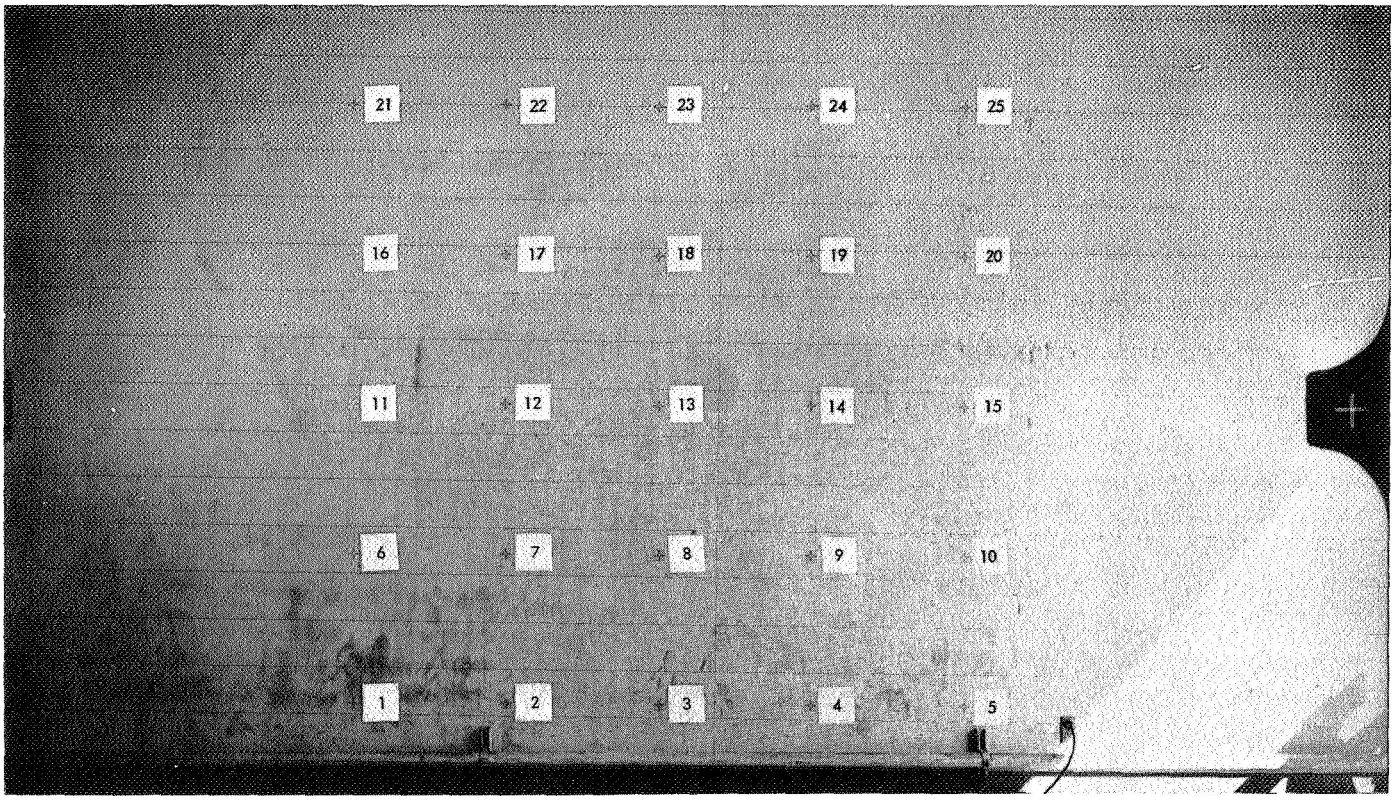

Fig. 9. Test grid

meter scale. The best standard error of one observation was ±0.06 mm, and the worst was ±0.15 mm, which is excellent.

Chosen was a right-handed coordinate system whose $\overline{XY}$ plane was identical with the test grid plane and whose Z-axis pointed from the center target toward the SMK-120 camera. In this manner, a redundant number of observations for a least-squares adjustment of the X and Y grid coordinates was obtained.

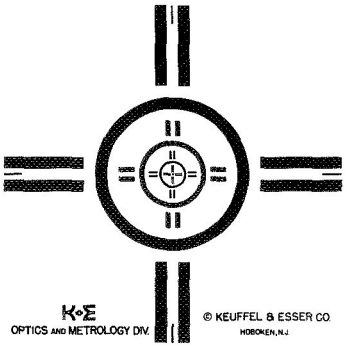

Fig. 10. Alignment target

The distance between any two targets i and j can be computed from:

$$s_{i,j} = [(X_i - X_j)^2 + (Y_i - Y_j)^2]^{1/2} \tag{13}$$

This, of course, is a true ideal condition that can never be satisfied. Instead, observed, approximate, and residual values must be introduced, which results in an observation equation:

$$s^o_{i,j} + v_{i,j} = \{[(X^a_i + \Delta X_i) - (X^a_j + \Delta X_j)]^2 + [(Y^a_i + \Delta Y_i) - (Y^a_j + \Delta Y_j)]^2\}^{1/2} \tag{14}$$

where

$s^o_{i,j}$ = observed (measured) distance between two grid points i and j

$v_{i,j}$ = residual observational error resulting from least-squares adjustment

$X^a_i, Y^a_i, X^a_j, Y^a_j$ = approximate values of unknown grid coordinates of points i and j

$\Delta X_i, \Delta Y_i, \Delta X_j, \Delta Y_j$ = corrections to the assumed approximate values

These equations must be further reduced by applying the Taylor's series expansion. Linearized observation equations of the following type are obtained:

$$v_{i,j} = p_1\Delta X_i + p_2\Delta Y_i + p_3\Delta X_j + p_4\Delta Y_j + \ell_{i,j} \tag{15}$$

where

$$\ell_{i,j} = [(X_i^a - X_j^a)^2 + (Y_i^a - Y_j^a)^2]^{1/2} - s_{i,j}^o = s_{i,j}^a - s_{i,j}^o$$

$$p_1 = \frac{X_i^a - X_j^a}{s_{i,j}^a}$$

$$p_2 = \frac{Y_i^a - Y_j^a}{s_{i,j}^a}$$

$$p_3 = -p_1$$

$$p_4 = -p_2$$

If all measured distances are used a complex system of observation equations is used that can be written in a compact matrix form:

$$\mathbf{V} = \mathbf{P}\Delta = \mathbf{L} \tag{16}$$

The least-squares solution of these equations is based on the requirement that the weighted sum of the squares of the residual errors is equal to minimum, i.e.:

$$\mathbf{V}^T\mathbf{W}\mathbf{V} = \min \tag{17}$$

Equation (17) can be differentiated with respect to the individual unknown parameters, which results in a system of normal equations:

$$\mathbf{N}\Delta = \mathbf{U} \tag{18}$$

where

$$\mathbf{N} = \mathbf{P}^T\mathbf{W}\mathbf{P}$$

$$\mathbf{U} = -\mathbf{P}^T\mathbf{W}\mathbf{L}$$

The computational process naturally is an iterative one, and, if μ is the standard error of unit weight after the final iteration, the variance–covariance matrix of the adjusted grid coordinates can be computed from:

$$\mathbf{M}^2 = \mathbf{N}^{-1}\mu^2 \tag{19}$$

A FORTRAN program was written for this purpose, and the resulting standard error of unit weight was ± 0.09 mm, which corresponds to approximately 0.002% of the camera distance.

The Z-coordinates of the test grid were read on the same steel meter scale with a theodolite pointed parallel with the $\overline{XY}$ plane. The resulting average standard error was ± 0.12 mm, which corresponds to 0.0027% of the camera distance.

The test grid can thus be considered as absolutely perfect for the given objectives because its coordinate accuracy considerably exceeds the observational accuracy of the test itself.

Another problem was that commercially produced cameras of this type usually do not have calibrated fiducial marks; however, with a Mann monocomparator they were measured on all exposed plates and the same trilateration method as described earlier enabled their reliable least-squares adjustment with a resulting average standard error of less than ± 1 μm.

The video film converter was not equipped to accommodate image formats of the given size and it was, therefore, necessary to use reduced images. The rate of reduction was chosen in such a way that image resolution of approximately 0.025 mm (i.e., 40 line pairs/mm) was obtained. This corresponds very well to conditions of regular vidicon photography; however, because of image format reduction, the object resolution measured in the test grid plane was rather low.

B. Results

Consequently, the conclusions stated herein must be considered as pertaining to the worst low-resolution cases, particularly the 600-line scan mode, whereas high resolution photography can be expected to produce proportionately better results.

As was mentioned earlier, the basic objective of this test was to define the detrimental effect of TV photography upon the mapping accuracy. This was done by comparing the observational and absolute orientation accuracies.

1. Comparison of observational accuracy. Ten different pictures of the test grid were taken with the SMK-120 camera and the obtained glass plates were converted to simulated TV pictures using 1000- and 600-line scan modes. Each of these was then observed several times on a Mann monocomparator; the method enabled a compar-

ison of observational accuracy between corresponding grid points.

However, one additional problem was encountered in the converted TV images. The general quality of these pictures was poor, but digital image processing was applied and the final pictures were enhanced to an excellent level of clarity and detail.

This in itself proves how important digital image processing is, although only contrast enhancement was used and no attempt was made to improve or eliminate geometric distortions.

The four previously calibrated fiducial marks were used for transformation of the observed image coordinates into the camera system. Normal affine transformation was used:

$$\bar{x} = x + a_1 x + b_1 y + c_1$$
$$\bar{y} = y + a_2 x + b_2 y + c_2 \qquad (20)$$

where

x, y = observed image coordinates

$\bar{x}, \bar{y}$ = transformed image coordinates

$a_1, b_1, c_1, a_2, b_2 c_2$ = transformation parameters resulting from least-squares adjustment

The results obtained are summarized in Table 7, which shows averaged standard errors of unit weight resulting from affine transformation for the fiducial marks and averaged standard observational errors for measured grid points.

It can clearly be seen from this table that the detrimental effect of TV photography is quite large. On the other hand, there does not seem to be too much difference between the 1000- and 600-line scan TV modes insofar as image point accuracy is concerned. However, the given numbers do not provide complete information because they do not relate anything about outliers (i.e., points that could not be measured at all, or that were eliminated because their observational accuracy was unacceptable). In fact, there were a few of these points in both the 1000- and 600-line scan TV pictures, and their number was much larger in the latter case.

Another interesting phenomenon is that, compared to the observed points, the fiducial marks have larger

Table 7. Comparison of observational accuracy

Observed point	Averaged standard error, μm		
	SMK-120 camera	1000-line scan TV picture	600-line scan TV picture
Fiducial marks	±3.2	±9.2	±41.7
X-coordinates	±1.9	±7.1	±11.1
Y-coordinates	±2.3	±8.6	±12.2

standard errors and their accuracy decrease is much sharper. This can be explained in part by the way the fiducial marks were calibrated (i.e., regardless of the precautions and care that are taken, the trilateration method cannot supply as good results as factory calibration); however, these differences are insignificant.

These anomalies can be explained principally by the presence of optical, photometric, and electronic aberrations, as well as by geometric distortions, that evidently can assume very large values. In the interest of mapping accuracy, it is, therefore, necessary to confront these difficulties and to eliminate their influences, or at least considerably reduce them.

One way to do this would be to develop and construct larger vidicons with higher resolution and lower aberrations and distortions. Until this is done, however, it will be necessary to fully utilize the benefits of digital image processing and to give more attention to residual geometric distortions. Some of these problems and their aspects are discussed in Section VII.

2. Comparison of absolute orientation accuracy. Using the same SMK-120 pictures that were used in the comparison of observational accuracy, three different stereomodels of the test grid were evaluated for accuracy comparison purposes.

The SMK-120 camera represents a fixed orientation system widely used in terrestrial photogrammetry, which enables a simple computation of model coordinates:

$$Z = -b \frac{f}{p_x} \qquad (21)$$

$$X = -Z \frac{x'}{f} \qquad (22)$$

$$Y = -Z \frac{y'}{f} \qquad (23)$$

where

b = stereophotogrammetric base ($b = 1200$ mm in this particular case)

f = focal length (for SMK-120, $f = 60$ mm)

x', y' = observed image coordinates of a target point measured on the left plate

p_x = horizontal parallax

Based on different image observations, this was done several times for all three pertinent cases: the SMK-120 camera and the 1000- and 600-line scan TV pictures.

Equations (21–23) usually are sufficient for any practical purposes; however, experience has shown that in many cases residual aberrations and imperfections of the fixed stereometric camera system can be improved by using the normal relative orientation approach. It was decided, therefore, to use this method as well (its description can be found in Refs. 1 or 2 or in any basic photogrammetric manual).

In the next step, the obtained stereomodel coordinates, both from Eqs. (21–23) and from relative orientation adjustment, were transformed into the given test grid coordinate system by using the method of absolute orientation.

Generally speaking, transformation from one system into another—in this case, from the test grid system into the stereomodel one and vice versa—is a function of three rotations, three translations, and a scale factor that can be written in a simple matrix form:

$$X_M = s\,\mathbf{A}X_G + \mathbf{B} \tag{24}$$

where

X_M = stereomodel coordinates

s = scale factor

$\mathbf{A}$ = rotational matrix going from ground into model system

X_G = given test grid coordinates

$\mathbf{B}$ = translational vector

and for the reversed final transformation:

$$X_G = \frac{1}{s}\mathbf{A}^T[X_M - \mathbf{B}] \tag{25}$$

This, of course, is, again, an iterative least-squares adjustment problem involving seven unknown parameters. As before, let a denote approximate values and o observed values; then Eq. (24) can be reduced to the familiar observation equation form:

$$\mathbf{V} + X_M^0 = (s\mathbf{A}X_G + \boldsymbol{B})^a + d(s\mathbf{A}X_G + \boldsymbol{B})^a \tag{26}$$

or

$$\mathbf{V} = \mathbf{L} + \mathbf{P}\Delta \tag{26a}$$

Solution of this system of observation equations is the same as was shown in Eqs. (17–19); however, after the unknown seven parameters are determined, Eq. (25) must still be used for the actual transformation from the model system into the test grid system.

The statistical results of this test are shown in Table 8, which gives the averaged values of resulting standard errors of unit weight, as well as their corresponding percentages with respect to the object distance.

Table 8. Comparison of absolute orientation accuracy

Parameter	Image		
	SMK-120 camera	1000-line scan TV picture	600-line scan TV picture
Terrestial photogrammetry			
Averaged value of resulting standard errors of unit weight, mm	0.5	2.2	3.5
Corresponding percentage with respect to object distance, %	0.011	0.048	0.078
Relative orientation			
Averaged value of resulting standard errors of unit weight, mm	0.4	1.9	3.2
Corresponding percentage with respect to object distance, %	0.009	0.042	0.071

It is evident that a conclusion similar to that from Table 7 can be drawn from Table 8: the detrimental influence of TV photography upon final mapping accuracy is quite strong. The relatively small difference between the 1000- and 600-line scan mode results can again be explained by the number of eliminated outliers

(i.e., points that could not be used for absolute orientation least-squares adjustment).

In addition, it will be noticed that relative orientation actually yields slightly better results than the simpler method of terrestrial photogrammetry, which only confirms the general experience mentioned earlier.

It would be very interesting to compare these practical results with those of theoretical error analysis described in Section III, but, unfortunately, none of the stereomodels treated there can be considered as fully representative of the SMK-120 camera system. Nevertheless, Fig. 4c, which is closest to this particular combination, shows an amazing correlation between the theoretical and practical results. This, again, indirectly confirms that the derived error analysis is correct and also that the performed analog test was realistic.

C. Conclusions

Considering the original constraints of the TV converting procedure, it must not be forgotten that all these results are characteristic of low-resolution photography, so that high-resolution photography can be expected to produce somewhat better results. However, these most important conclusions pertaining to TV image quality and the resulting mapping accuracy can be repeated:

(1) Larger vidicon with higher resolution and lower aberrations and distortions is extremely desirable.

(2) Digital image-processing techniques should be utilized to their full capacity.

(3) Residual geometric distortions of the camera system should be calibrated and analytically eliminated.

VII. Interior Orientation Calibration

Photometric calibration of a TV camera system represents a complex problem that requires a combined intensive effort. It has been performed with success in the *Ranger*, *Surveyor*, and *Mariner* Projects.

However, from the photogrammetric point of view, only basic optical calibrations were obtained. This type of incomplete photogrammetric calibration may result in dangerous systematic or pseudo-systematic errors that unfavorably influence the mapping accuracy. These problems have been indicated and described several times in previous sections; however, it was considered necessary to devote a separate section to their detailed discussion.

The importance of a complex interior orientation calibration procedure (i.e., determination of the correct focal length, principal point eccentricity, and complex geometric distortions) is evident and it definitely should be integrated with the overall camera system calibration activity. These calibrations can be done either *optically* or *analytically*.

Optical calibration procedures have been widely and successfully used for this purpose for some time; however, they require the use of special optical benches with high-precision collimators and other expensive measuring devices. Moreover, their applicability to extraterrestrial TV cameras is somewhat limited. This makes the analytical approach, or at least a combination of both these methods, quite attractive and desirable.

A. Approach

One of the best and most comprehensive mathematical derivations of analytical calibration pertaining to TV photography can be found in Ref. 7. The results and conclusions contained therein were modified and extended to meet specific problems of this task, and a complex FORTRAN program was written to enable computation of all the required photogrammetric parameters. The solution is based on the principle of collinearity between the image and object planes; the latter is represented by an accurate test grid:

$$F_x = \begin{vmatrix} x & z \\ \mathbf{A}_1\mathbf{B} & \mathbf{A}_3\mathbf{B} \end{vmatrix} = 0 \tag{27}$$

$$F_y = \begin{vmatrix} y & z \\ \mathbf{A}_2\mathbf{B} & \mathbf{A}_3\mathbf{B} \end{vmatrix} = 0 \tag{28}$$

where

x, y = image coordinates corrected for the principal point eccentricity and the lens distortion influence

z = the negative focal length

$\mathbf{A}$ = the rotational matrix going from "ground" to "photo" using the X, Y, Z (ω, ϕ, κ) sequence of rotation, and

$$\mathbf{B} = \begin{bmatrix} X - X_0 \\ Y - Y_0 \\ Z - Z_0 \end{bmatrix} \tag{29}$$

is the translational vector between object plane points and camera system center of projection.

The problem now is to determine the optimum adjusted values of image coordinates x, y.

Figure 11 clearly shows the relation between correct coordinates x, y and observed coordinates $\bar{x}, \bar{y}$, as far as principal point eccentricity is concerned:

$$x = \bar{x} - x_P \tag{30}$$

$$y = \bar{y} - y_P \tag{31}$$

Equations (30) and (31) must now be further extended to express the lens-distortion influence.

There are basically two kinds of geometrical distortion: optical distortion and electronic distortion.

Electronic distortion can be numerically eliminated, or at least considerably reduced, if accurate reseau grid is available (see Section VI and Ref. 6), but optical and residual electronic distortion must be analytically defined. These problems are treated in detail in Ref. 7, and it was possible, therefore, to utilize the final conclusions contained therein.

Equations (30) and (31) can then be written as:

$$x = (\bar{x} - x_P)(1 + p_1 r^2 + p_2 r^4) - (\bar{y} - y_P) \times (q_1 r + q_2 r^3) - (t_1 r^2 + t_2 r^4) \sin \theta_0 \tag{30a}$$

$$y = (\bar{y} - y_P)(1 + p_1 r^2 + p_2 r^4) + (\bar{x} - x_P) \times (q_1 r + q_2 r^3) + (t_1 r^2 + t_2 r^4) \cos \theta_0 \tag{31a}$$

where

p_1, p_2 = coefficients defining symmetric radial distortion

q_1, q_2 = coefficients defining symmetric tangential distortion

t_1, t_2 = coefficients defining asymmetric radial and tangential distortion

θ_0 = angular distance of the axis of maximum asymmetric distortion, and

$r = [(\bar{x} - x_P)^2 + (\bar{y} - y_P)^2]^{1/2}$

is radial distance between the principal point and observed points

Equations (30a) and (31a) can be substituted into Eqs. (27) and (28), and, using the Taylor's series expansion, the following observation equations can be obtained:

$$\mathbf{C}_{(2\times2)}\mathbf{V}_{(2\times1)} + \mathbf{D}_{(2\times16)}\Delta_{(16\times1)} + \mathbf{E}_{(2\times1)} = 0 \tag{32}$$

where

$\mathbf{C}$ = coefficient matrix of observed image coordinates $\bar{x}, \bar{y}$

$\mathbf{V}$ = vector of $\bar{x}, \bar{y}$

$\mathbf{D}$ = coefficient matrix of unknown parameters

Δ = vector of unknown parameters

$\mathbf{E}$ = vector of constant terms

These 16 unknown parameters are involved in the process of least-squares adjustment:

Lens distortion coefficients p_1, p_2, q_1, q_2, t_1, and t_2

Angular distance θ_0

Principal point eccentricity x_P, y_P

Focal length z (i.e., its negative value)

Rotation ω, ϕ, κ

Coordinates of the center of projection X_0, Y_0, Z_0

The required coefficients c and d, as well as the constant terms e, can now be derived as follows:

If

$$\mathbf{A} = \begin{bmatrix} \cos\phi\cos\kappa & \cos\omega\sin\kappa + \sin\omega\sin\phi\cos\kappa & \sin\omega\sin\kappa - \cos\omega\sin\phi\cos\kappa \\ -\cos\phi\sin\kappa & \cos\omega\cos\kappa - \sin\omega\sin\phi\sin\kappa & \sin\omega\cos\kappa + \cos\omega\sin\phi\sin\kappa \\ \sin\phi & -\sin\omega\cos\phi & \cos\omega\cos\phi \end{bmatrix}$$

$$= \begin{bmatrix} a_{1,1} & a_{1,2} & a_{1,3} \\ a_{2,1} & a_{2,2} & a_{2,3} \\ a_{3,1} & a_{3,2} & a_{3,3} \end{bmatrix} = \begin{bmatrix} \mathbf{A}_1 \\ \mathbf{A}_2 \\ \mathbf{A}_3 \end{bmatrix}$$

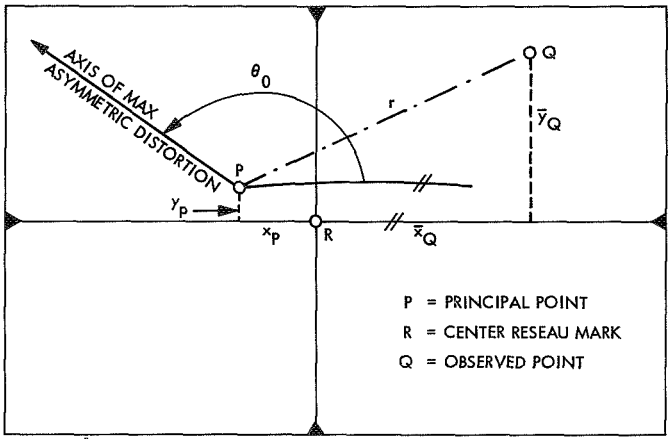

Fig. 11. Image plane geometry

$$c_{1,1} = \frac{\partial F_x}{\partial \bar{x}} = \mathbf{A}_3\mathbf{B}\,(1 + p_1 r^2 + p_2 r^4)$$

$$c_{1,2} = \frac{\partial F_x}{\partial \bar{y}} = -\mathbf{A}_3\mathbf{B}\,(q_1 r + q_2 r^3)$$

$$d_{1,1} = \frac{\partial F_x}{\partial p_1} = \mathbf{A}_3\mathbf{B}\,(\bar{x} - x_P)\,r^2$$

$$d_{1,2} = \frac{\partial F_x}{\partial p_2} = \mathbf{A}_3\mathbf{B}\,(\bar{x} - x_P)\,r^4$$

$$d_{1,3} = \frac{\partial F_x}{\partial q_1} = -\,\mathbf{A}_3\mathbf{B}\,(\bar{y} - y_P)\,r$$

$$d_{1,4} = \frac{\partial F_x}{\partial q_2} = -\,\mathbf{A}_3\mathbf{B}\,(\bar{y} - y_P)\,r^3$$

$$d_{1,5} = \frac{\partial F_x}{\partial t_1} = -\mathbf{A}_3\mathbf{B} r^2 \sin\theta_0$$

$$d_{1,6} = \frac{\partial F_x}{\partial t_2} = -\mathbf{A}_3\mathbf{B} r^4 \sin\theta_0$$

$$d_{1,7} = \frac{\partial F_x}{\partial \theta_0} = -\mathbf{A}_3\mathbf{B}\,(t_1 r^2 + t_2 r^4)\cos\theta_0$$

$$d_{1,8} = \frac{\partial F_x}{\partial x_P} = -\mathbf{A}_3\mathbf{B}\,(1 + p_1 r^2 + p_2 r^4)$$

$$d_{1,9} = \frac{\partial F_x}{\partial y_P} = \mathbf{A}_3\mathbf{B}\,(q_1 r + q_2 r^3)$$

$$d_{1,10} = \frac{\partial F_x}{\partial_z} = -\mathbf{A}_1\mathbf{B}$$

$$d_{1,11} = \frac{\partial F_x}{\partial \omega} = \begin{vmatrix} x & z \\ [0 \quad -a_{1,3} \quad a_{1,2}]\cdot\mathbf{B} & [0 \quad -a_{3,3} \quad a_{3,2}]\cdot\mathbf{B} \end{vmatrix}$$

$$d_{1,12} = \frac{\partial F_x}{\partial \phi} = \begin{vmatrix} x & z \\ \dfrac{\partial(\mathbf{A}_1\mathbf{B})}{\partial\phi} & \dfrac{\partial(\mathbf{A}_3\mathbf{B})}{\partial\phi} \end{vmatrix}$$

where

$$\frac{\partial(\mathbf{A}_1\mathbf{B})}{\partial\phi} = [-\sin\phi\cos\kappa \qquad \sin\omega\cos\phi\cos\kappa \qquad -\cos\omega\cos\phi\cos\kappa]\cdot\mathbf{B}$$

$$\frac{\partial(\mathbf{A}_3\mathbf{B})}{\partial\phi} = [\cos\phi \qquad \sin\omega\sin\phi \qquad -\cos\omega\sin\phi]\cdot\mathbf{B}$$

$$d_{1,13} = \frac{\partial F_x}{\partial \kappa} = \begin{vmatrix} x & z \\ [a_{2,1} \quad a_{2,2} \quad a_{2,3}]\cdot\mathbf{B} & 0 \end{vmatrix} = -z\,[a_{2,1} \quad a_{2,2} \quad a_{2,3}]\cdot\mathbf{B}$$

$$d_{1,14} = \frac{\partial F_x}{\partial X_0} = -\begin{vmatrix} x & z \\ a_{1,1} & a_{3,1} \end{vmatrix}$$

$$d_{1,15} = \frac{\partial F_x}{\partial Y_0} = -\begin{vmatrix} x & z \\ a_{1,2} & a_{3,2} \end{vmatrix}$$

$$d_{1,16} = \frac{\partial F_x}{\partial Z_0} = -\begin{vmatrix} x & z \\ a_{1,3} & a_{3,3} \end{vmatrix}$$

$$e_1 = \begin{vmatrix} x & z \\ \mathbf{A}_1\mathbf{B} & \mathbf{A}_3\mathbf{B} \end{vmatrix}$$

and, similarly, for the F_y function:

$$c_{2,1} = \frac{\partial F_y}{\partial \bar{x}} = \mathbf{A}_3\mathbf{B}\,(q_1 r + q_2 r^3) = -c_{1,2}$$

$$c_{2,2} = \frac{\partial F_y}{\partial \bar{y}} = \mathbf{A}_3\mathbf{B}\,(1 + p_1 r^2 + p_2 r^4) = c_{1,1}$$

$$d_{2,1} = \frac{\partial F_y}{\partial p_1} = \mathbf{A}_3\mathbf{B}\,(\bar{y} - y_P)\,r^2$$

$$d_{2,2} = \frac{\partial F_y}{\partial p_2} = \mathbf{A}_3\mathbf{B}\,(\bar{y} - y_P)\,r^4$$

$$d_{2,3} = \frac{\partial F_y}{\partial q_1} = \mathbf{A}_3\mathbf{B}\,(\bar{x} - x_P)\,r$$

$$d_{2,4} = \frac{\partial F_y}{\partial q_2} = \mathbf{A}_3\mathbf{B}\,(\bar{x} - x_P)\,r^3$$

$$d_{2,5} = \frac{\partial F_y}{\partial t_1} = \mathbf{A}_3\mathbf{B}r^2 \cos\theta_0$$

$$d_{2,6} = \frac{\partial F_y}{\partial t_2} = \mathbf{A}_3\mathbf{B}r^4 \cos\theta_0$$

$$d_{2,7} = \frac{\partial F_y}{\partial \theta_0} = -\mathbf{A}_3\mathbf{B}\,(t_1 r^2 + t_2 r^4) \sin\theta_0$$

$$d_{2,8} = \frac{\partial F_y}{\partial x_P} = -\mathbf{A}_3\mathbf{B}\,(q_1 r + q_2 r^3) = -d_{1,9}$$

$$d_{2,9} = \frac{\partial F_y}{\partial y_P} = -\mathbf{A}_3\mathbf{B}\,(1 + p_1 r^2 + p_2 r^4) = d_{1,8}$$

$$d_{2,10} = \frac{\partial F_y}{\partial z} = -\mathbf{A}_2\mathbf{B}$$

$$d_{2,11} = \frac{\partial F_y}{\partial \omega} = \begin{vmatrix} y & & & z & & \\ [0 & -a_{2,3} & a_{2,2}] \cdot \mathbf{B} & [0 & -a_{3,3} & a_{3,2}] \cdot \mathbf{B} \end{vmatrix}$$

$$d_{2,12} = \frac{\partial F_y}{\partial \phi} = \begin{vmatrix} y & z \\ \dfrac{\partial(\mathbf{A}_2\mathbf{B})}{\partial\phi} & \dfrac{\partial(\mathbf{A}_3\mathbf{B})}{\partial\phi} \end{vmatrix}$$

where

$$\frac{\partial(\mathbf{A}_2\mathbf{B})}{\partial\phi} = [\sin\phi\sin\kappa \quad -\sin\omega\cos\phi\sin\kappa \quad \cos\omega\cos\phi\sin\kappa]\cdot\mathbf{B}$$

$$\frac{\partial(\mathbf{A}_3\mathbf{B})}{\partial\phi} = [\cos\phi \quad \sin\omega\sin\phi \quad -\cos\omega\sin\phi]\cdot\mathbf{B}$$

$$d_{2,13} = \frac{\partial F_y}{\partial\kappa} = \begin{vmatrix} & y & & z \\ [-a_{1,1} & -a_{1,2} & -a_{1,3}]\cdot\mathbf{B} & 0 \end{vmatrix} = -z[-a_{1,1} \quad -a_{1,2} \quad -a_{1,3}]\cdot\mathbf{B}$$

$$d_{2,14} = \frac{\partial F_y}{\partial X_0} = -\begin{vmatrix} y & z \\ a_{2,1} & a_{3,1} \end{vmatrix}$$

$$d_{2,15} = \frac{\partial F_y}{\partial Y_0} = -\begin{vmatrix} y & z \\ a_{2,2} & a_{3,2} \end{vmatrix}$$

$$d_{2,16} = \frac{\partial F_y}{\partial Z_0} = -\begin{vmatrix} y & z \\ a_{2,3} & a_{3,3} \end{vmatrix}$$

$$e_2 = \begin{vmatrix} y & z \\ \mathbf{A}_2\mathbf{B} & \mathbf{A}_3\mathbf{B} \end{vmatrix}$$

Similarly, as in the trilateration case (Eqs. (16–18)), solution of observation Eq. (32) is based on the same least-squares requirement; i.e.,

$$\mathbf{V}^T\mathbf{W}\mathbf{V} = \min \qquad (33) \equiv (16)$$

which leads to a familiar system of normal equations:

$$\mathbf{N}\Delta = \mathbf{U} \qquad (34) \equiv (17)$$

where

$$\mathbf{N} = \mathbf{D}^T\mathbf{W}\mathbf{D}$$

$$\mathbf{U} = -\mathbf{D}^T\mathbf{W}\mathbf{E}$$

However, determination of the weight matrix $\mathbf{W}$ is somewhat more complicated than before because there are two observed quantities in each observation equation instead of the usual one; i.e.,

$$\mathbf{W} = [\mathbf{C}\mathbf{W}_0^{-1}\mathbf{C}^T]^{-1} \qquad (35)$$

where $\mathbf{W}_0$ is the weight matrix of the observed image coordinates $\bar{x}$ and $\bar{y}$ (in most cases $\mathbf{W}_0 = I$).

The whole process, naturally, is an iterative one and several iterations are always required before all Δ expressions start converging toward zero. After the final iteration, Eq. (19) can again be used for computation of the variance–covariance matrix of the adjusted parameters.

All original starting values can be chosen as equal to zero, except for f, X_0, Y_0, and Z_0, which are always known with a sufficient degree of accuracy. However, special attention must be paid to parameters t_1 and θ_0. In the case of a very small or zero asymmetric distortion, which is the most likely case, these two parameters can easily result in an indeterminate system of normal equations. It is, therefore, necessary to:

(1) Assign some starting value to parameter t_1, either from experience or from trial runs.

(2) Treat θ_0 as an observed quantity by adding a simple observation equation with a very small weight factor. (If desired, a similar procedure can be applied to coordinates X_0, Y_0, and Z_0 as well, but it is not necessary.)

B. Results and Conclusions

1. Theoretical tests. A series of numerical tests based on hypothetical fictitious models was performed to verify the usefulness and applicability of this method.

At least nine test grid points are required for a least-squares fit; however, a larger number should be used for a more reliable adjustment.

a. Approach. The basic idea of the test was very simple. Known calibration inaccuracies and distortions were introduced into the assumed fictitious models, and the corresponding image coordinates were gradually changed in a random fashion. Using the described method, the resulting adjusted parameters were then compared with their hypothetical correct values. The same image formats as before (i.e., small vidicon, large vidicon, *Lunar Orbiter*, and large format) were used.

b. Results. Generally speaking, the obtained results were excellent, particularly for larger formats and/or smaller focal lengths. However, for very narrow-angle photography, the differences became larger as did the standard errors of these adjusted parameters. In some cases, mainly for the small-vidicon photography, the least-squares adjustment had a tendency to result in an ill-conditioned system of normal equations that either gave an unrealistic solution or failed to converge at all.

These results are unfortunate, but only to a certain degree. It will be remembered from the discussion in Section V that calibration requirements can be reduced considerably, or even eliminated, if very narrow-angle photography is used. This conclusion is, of course, very fortunate from the calibration procedure standpoint and should always be remembered before any accuracy criteria and limits are set.

c. Conclusions. The investigations performed and their pertinent conclusions may be summarized as follows:

(1) The theoretical background of this method, as well as its mathematical derivation, is correct. In most cases, the theory and its derivation can successfully and effectively be used for a complex photogrammetric calibration of the given camera system.

(2) The test grid used should contain at least nine points, but an increased number will provide better and more reliable results. On the other hand, more than 50 points should not be used either, because, in this case, the obtained accuracy increase is not commensurate with the tremendously increased numerical effort. Test grid of 25 points can, therefore, be recommended as an optimum solution.

d. Solution of difficulties. When the aforementioned numerical difficulties connected with narrow-angle photography occur, some of the following steps, or combinations of these steps, can be taken to facilitate the solution:

(1) Separate observation equations for X_0, Y_0, and Z_0 coordinates of the center of projection can be added with assigned low weight factors (similarly as for θ_0).

(2) On the other hand, rotations ω, ϕ, and κ can eventually be treated as constants if their approximate values are reasonably well known. Experience usually has shown that these parameters may act as strong diverging factors, whereas their omission cannot significantly influence the adjusted values of the other parameters.

(3) Combined optical and analytical calibration procedures should be used; e. g., the optical approach can conveniently be used for determination of the focal length and the principal point eccentricity, whereas the analytical method would be used for geometric distortions only. (There are, of course, a few other combinations or modifications that may be applied instead of the one mentioned here.)

(4) The best solution of this problem, however, seems to be that of an extensive and consistent utilization of digital image processing techniques combined with the analytical method described earlier; i.e., digital image processing can be used not only for general image quality enhancement, but also for elimination of electronic distortions, whereas residual optical distortions and remaining unknown parameters can then be determined analytically.

2. Practical tests. To complete this study, a series of practical tests, in addition to the theoretical investigations described earlier, was performed. The purpose of these tests was two-fold: (1) to apply the designed analytical calibration method to a real camera system, and (2) similarly, as noted in the previous section, to define the detrimental effect of TV photography upon the image quality.

a. Approach. The Zeiss SMK-120 stereometric camera and the test grid (see Fig. 9) described in Section VI were used. Thus, the general assumptions and conclusions described therein pertain to this test as well.

b. Results. The results of this test are shown in Table 9. The manufacturer claims that both SMK-120 cameras are essentially distortion-free; the focal lengths are defined as $f_L = 60.44$ mm and $f_R = 60.40$ mm (left and right, respectively). No information is supplied concerning

Table 9. Comparison of interior orientation calibration results

Parameter	Image	
	SMK-120 camera	1000-line scan TV picture
Focal length, mm		
Left	60.455 ±0.018	60.466 ±0.044
Right	60.433 ±0.011	60.335 ±0.037
Computed zero principal point eccentricity x_P, mm		
Left	−0.136 ±0.020	−0.228 ±0.049
Right	0.154 ±0.012	0.062 ±0.040
Computed zero principal point eccentricity y_P, mm		
Left	0.035 ±0.020	0.139 ±0.049
Right	−0.018 ±0.012	0.025 ±0.040

principal point eccentricity, which suggests that it should be nonexistent.

It is very interesting to analyze the results obtained. The calibrated distortions were really insignificant and, therefore, were not even mentioned in Table 9. The average calibrated values of the focal lengths were f_L = 60.455 ±0.018 mm and f_R = 60.433 ±0.011 mm, which correspond very well to the given values. However, the assumed zero principal point eccentricities were calibrated to be as high as 0.154 mm. This may seem surprising, but, in reality, it only confirms that not enough attention had been paid to these important photogrammetric parameters. These parameters can, at least to a certain extent, be neglected when sufficient ground control points are available, but definitely not in extraterrestrial photogrammetry (see also Section V).

These calibrated parameters were also used for computation of the same stereomodels as discussed in Section VI. It is interesting to note that the resulting absolute orientation accuracy was considerably improved as a result. In the case of a fixed orientation camera system, the increase was from 0.5 mm/0.011% to 0.18 mm/0.004%, and for relative orientation, from 0.4 mm/0.009% to 0.14 mm/0.003%. This is another proof that interior orientation calibration should always be performed and that the designed analytical method is capable of achieving this goal.

c. Conclusions. As was the case with Table 8, Table 9 clearly illustrates the detrimental effect of TV photography upon image quality and its correlated measuring accuracy. The 1000-line scan TV models yielded a solution, although of a somewhat doubtful value, whereas, because of many outliers and generally poor image quality, the 600-line scan TV models could not be used at all.

Fortunately, this drawback can be overcome by a separate optical and electronic distortion calibration, as has been mentioned. For very narrow-angle cameras, all measurements can be performed directly in the vidicon image plane without the necessity of taking any pictures of the test target. Another possible approach would be to use the vidicon target as an object plane and observe it through the lens, but this would require certain additional modifications of the mathematical relations given here. However, these results undeniably confirm the final conclusions enumerated in the previous section, and all efforts should be made to ensure their practical implementation in future space-mapping missions.

VIII. Conclusions

This report cannot claim to have solved all the aspects connected with the given problem. However, it is believed that the long-range objective of this project (i.e., definition of specific photogrammetric parameters that could be incorporated into an extraterrestrial television mapping system) has been achieved.

On the basis of experience, the research was devoted mainly to investigations of convergent photogrammetric stereomodels. An extensive error analysis of direct and external relative orientation was performed and described. Considerable attention was also paid to systematic influences of interior orientation calibration errors.

These theoretical investigations were supplemented by two practical tests. The first test investigated some aspects of TV image quality and its resulting influence upon the mapping accuracy, whereas the purpose of the second test was to design an effective analytical method for the complex interior orientation calibration.

It is expected that application of the resulting conclusions will enable an improved mapping capability in future missions.

References

1. Benes, M., "Complete Error Analysis of Relative and Absolute Orientation in Extraterrestrial Mapping Techniques," in *Supporting Research and Advanced Development,* Space Programs Summary 37-45, Vol. IV, pp. 209–221. Jet Propulsion Laboratory, Pasadena, Calif., June 30, 1967.

2. Benes, M., "Relative and Absolute Orientation Error Analysis," *Photogram. Eng.,* Nov. 1968. Also available as Technical Report 32-1344, Jet Propulsion Laboratory, Pasadena, Calif., Nov. 1968.

3. Keller, M., and Tewinkel, G. C., *Three-Photo Aerotriangulation,* Technical Bulletin No. 29. U.S. Coast and Geodetic Survey, Feb. 1966.

4. Moellman, D. E., *A Comparative Study of Two-Photo Versus Three-Photo Relative Orientation,* Civil Engineering Studies, Photogrammetry Series No. 7. University of Illinois, Urbana, Ill., Oct. 1967.

5. Benes, M., "Orbital Photogrammetric Mapping System," in *Supporting Research and Advanced Development,* Space Programs Summary 37-56, Vol. III, pp. 42–47. Jet Propulsion Laboratory, Pasadena, Calif., Apr. 30, 1969.

6. Efron, E., "Image Processing by Digital Systems," *Photogram. Eng.,* Oct. 1968.

7. Wong, K. W., *Photogrammetric Quality of Television Pictures,* Civil Engineering Studies, Photogrammetry Series No. 17. University of Illinois, Urbana, Ill., Feb. 1968.

NASA — JPL — Coml., L.A., Calif.

N71-19021

TECHNICAL REPORT STANDARD TITLE PAGE

1. Report No. 33-455	2. Government Accession No.	3. Recipient's Catalog No.
4. Title and Subtitle EXTRATERRESTRIAL CONVERGENT PHOTOGRAMMETRIC MAPPING SYSTEM--AN ERROR ANALYSIS		5. Report Date December 1, 1970 6. Performing Organization Code
7. Author(s) Milosh Benesh		8. Performing Organization Report No.
9. Performing Organization Name and Address JET PROPULSION LABORATORY California Institute of Technology 4800 Oak Grove Drive Pasadena, California 91103		10. Work Unit No. 11. Contract or Grant No. NAS 7-100 13. Type of Report and Period Covered Technical Memorandum
12. Sponsoring Agency Name and Address NATIONAL AERONAUTICS AND SPACE ADMINISTRATION Washington, D.C. 20546		14. Sponsoring Agency Code

15. Supplementary Notes

16. Abstract

An effort to define specific photogrammetric parameters that could be incorporated into an extraterrestrial television mapping system through investigations of convergent photogrammetric steromodels is described. Also described are error analyses of direct and external relative orientation, and practical tests that investigated: (1) aspects of TV image quality and its resulting influence upon mapping accuracy, and (2) the design of an effective analytical method for complex interior orientation calibration.

17. Key Words (Selected by Author(s))	18. Distribution Statement
Control and Guidance Mariner Mars 1971 Project Optics Photography	Unclassified -- Unlimited

19. Security Classif. (of this report)	20. Security Classif. (of this page)	21. No. of Pages	22. Price
Unclassified	Unclassified	38	

HOW TO FILL OUT THE TECHNICAL REPORT STANDARD TITLE PAGE

Make items 1, 4, 5, 9, 12, and 13 agree with the corresponding information on the report cover. Use all capital letters for title (item 4). Leave items 2, 6, and 14 blank. Complete the remaining items as follows:

3. Recipient's Catalog No. Reserved for use by report recipients.

7. Author(s). Include corresponding information from the report cover. In addition, list the affiliation of an author if it differs from that of the performing organization.

8. Performing Organization Report No. Insert if performing organization wishes to assign this number.

10. Work Unit No. Use the agency-wide code (for example, 923-50-10-06-72), which uniquely identifies the work unit under which the work was authorized. Non-NASA performing organizations will leave this blank.

11. Insert the number of the contract or grant under which the report was prepared.

15. Supplementary Notes. Enter information not included elsewhere but useful, such as: Prepared in cooperation with... Translation of (or by)... Presented at conference of... To be published in...

16. Abstract. Include a brief (not to exceed 200 words) factual summary of the most significant information contained in the report. If possible, the abstract of a classified report should be unclassified. If the report contains a significant bibliography or literature survey, mention it here.

17. Key Words. Insert terms or short phrases selected by the author that identify the principal subjects covered in the report, and that are sufficiently specific and precise to be used for cataloging.

18. Distribution Statement. Enter one of the authorized statements used to denote releasability to the public or a limitation on dissemination for reasons other than security of defense information. Authorized statements are "Unclassified—Unlimited," "U. S. Government and Contractors only," "U. S. Government Agencies only," and "NASA and NASA Contractors only."

19. Security Classification (of report). NOTE: Reports carrying a security classification will require additional markings giving security and downgrading information as specified by the Security Requirements Checklist and the DoD Industrial Security Manual (DoD 5220.22-M).

20. Security Classification (of this page). NOTE: Because this page may be used in preparing announcements, bibliographies, and data banks, it should be unclassified if possible. If a classification is required, indicate separately the classification of the title and the abstract by following these items with either "(U)" for unclassified, or "(C)" or "(S)" as applicable for classified items.

21. No. of Pages. Insert the number of pages.

22. Price. Insert the price set by the Clearinghouse for Federal Scientific and Technical Information or the Government Printing Office, if known.